PHYSICAL REVIEW D VOLUME 45, NUMBER 6 15 MARCH 1992

ARTICLES

Strong-field tests of relativistic gravity and binary pulsars

Thibault Damour
Institut des Hautes Etudes Scientifiques, 91440 Bures-sur-Yvette, France
and Département d'Astrophysique Relativiste et de Cosmologie, Observatoire de Paris, Centre National de la Recherche Scientifique, 92195 Meudon Cedex, France

J. H. Taylor
Joseph Henry Laboratories and Physics Department, Princeton University, Princeton, New Jersey 08544
(Received 10 September 1991)

Observations of pulsars in gravitationally bound binary systems provide a unique opportunity for testing the strong-field regime of relativistic gravity. We present a detailed account of the "parametrized post-Keplerian" (PPK) formalism, a general phenomenological framework designed to extract the maximum possible information from pulsar timing and pulse-structure data. The PPK approach allows dynamical information to be obtained from the data in a theory-independent way, and encoded in a certain number of fitted post-Keplerian parameters. We show that as many as 19 such parameters can be measured, under favorable conditions, giving access to 15 possible tests of relativistic gravity. We isolate and quantify the theoretical content of these tests by deriving, within the framework of generic boost-invariant theories, expressions linking the phenomenological parameters to the inertial masses of the pulsar and its companion, and to the polar angles of the spin axis of the pulsar. The prospects for extracting some of these tests from observations of known or yet-to-be-discovered binary pulsars is quantitatively assessed through numerical simulations. We show that the recently discovered binary pulsar PSR 1534+12 should, with presently available data, give access to two new strong-field tests of relativistic gravity, if the data are analyzed in the phenomenological way emphasized in this paper. Moreover, in the long run, the first-discovered binary pulsar, PSR 1913+16, could give access to three strong-field tests, beyond the presently obtained $\dot{\omega}$-γ-$\dot{P}_b$ test. Finally, we show how, by combining the PPK approach with the predictions of a rather generic class of tensor-biscalar theories, one can bring together tests based on observations of several different pulsars. We illustrate how such a combination of independent tests can lead to very tight quantitative constraints on possible strong-field deviations from the correct theory of gravity.

PACS number(s): 04.80.+z, 95.30.Sf, 97.60.Gb

I. INTRODUCTION

The discovery of binary pulsars in 1974 [1] opened up an entirely new testing ground for relativistic gravity. Up to their discovery, and apart from the qualitatively fascinating but quantitatively poor confirmations of general relativity coming from cosmological data, the only available testing ground for relativistic gravity was the solar system. Starting in the late 1950s, a favorable situation involving the availability of new technologies (including the Mössbauer effect, radar and laser ranging to solar-system bodies, atomic clocks, ...), and the conception of new tests of relativistic gravity [2–8], led to an intensive period of research in experimental gravity. From a theoretical point of view, the planning and interpretation of experimental tests was greatly assisted by two different but complementary approaches: on the one hand, the existence of a specific, theoretically well-motivated, one-parameter family of alternative theories of gravity, originally due to Jordan [9] and Fierz [10], and further developed by Brans and Dicke [11]; and on the other hand, the development of a general phenomenological framework, the parametrized post-Newtonian (PPN) formalism [12–15], able to describe with a minimum of theoretical assumptions the many directions in which very generic alternative theories of gravity might differ in their predictions from general relativity. The main conclusion one can draw from all the experimental results about solar-system gravity is that, within the assumptions of the PPN framework (notably the absence of any specific length scale in the gravitational interaction), the limiting regime of weak and quasistationary gravitational fields has been fairly completely mapped out at the first post-Newtonian level, i.e., when taking into account fractional corrections of order $(v/c)^2 \sim GM/c^2R$ to a Newtonian description of gravity, and found to agree with general relativity within a fractional accuracy of about 2×10^{-3} [16, 17].

In spite of the impressive quantitative value of solar-system tests, their qualitative value seems relatively limited when one considers that studying the behavior of the gravitational interaction in the combined weak-field-quasistationary ("post-Newtonian") limit is somewhat

similar to studying the behavior of a function, say $f(x)$, in a small neighborhood of one point, say $x = 0$. Seen from this point of view, the general PPN expansion is analogous to parametrizing, near $x = 0$, the behavior of a general class of functions by means, say, of a parabolic approximation, $f(x) = \alpha + \beta x + \gamma x^2 + O(x^3)$. Clearly such a local parametrization of $f(x)$ is unable to distinguish among functions which approximate each other closely at $x = 0$, but behave very differently in general. And indeed, the PPN formalism has provided several specific examples of theories, e.g., Rosen's bimetric theory, which approximate general relativity in the post-Newtonian regime while leading to very different predictions in the strong-field and/or rapidly-varying-field regimes [16].

Fortunately, the continuous observational study of the binary pulsar PSR 1913+16 [18–23] has provided us with a new laboratory for studying relativistic gravity. The distinguishing feature of this laboratory with respect to the solar-system one is that, since the pulsar and its companion are believed to be neutron stars, i.e., objects with more than a solar mass of material compressed within a radius of about 10 km, we have, for the first time, data about a system which contains some strong gravitational-field regions (surface fields $GM/c^2R \simeq 0.2$, as compared to $\sim 10^{-6}$ for the Sun). Moreover, the high stability of the pulsar clock has made it possible to monitor the dynamics of its orbital motion down to a precision where extremely small effects, $(v/c)^5$ times smaller than the main gravitational attraction, show up as gravitational radiation damping. At present the coherent recording over sixteen years of pulse arrival times from PSR 1913+16 has provided data which are very well fitted by a phenomenological, i.e., theory-independent, timing model (called below BT+) comprising, in addition to the expected "Keplerian" parameters (notably, the orbital period P_b, the eccentricity e, and the projected semimajor axis of the pulsar orbit $x \equiv a_1 \sin i/c$), three "post-Keplerian" parameters: the secular advance of the periastron, $\dot{\omega}$, a time dilation parameter γ, and the secular change of the orbital period, $\dot{P}_b$.

Any given relativistic theory of gravity makes a specific prediction for the values of $\dot{\omega}$, γ, and $\dot{P}_b$ as functions of the Keplerian parameters and the (*a priori* unknown) inertial masses m_1 and m_2 of the pulsar and its companion. In graphical terms, the phenomenological measurement of each post-Keplerian (PK) parameter in the set $\dot{\omega}$, γ, and $\dot{P}_b$ defines (when interpreted within the framework of a specific theory of gravity) a curve in the m_1, m_2 plane. It follows that simultaneous measurement of all three PK parameters yields one test of the theory, according to whether the three corresponding curves meet at one point, as they should. As first announced in 1979 [19], and confirmed with ever increasing accuracy as more data were accumulated [20–23], general relativity passes this $\dot{\omega}$-γ-$\dot{P}_b$ test with flying colors when using as the theoretical prediction for $\dot{P}_b$ a formula first obtained heuristically [24], and then derived more rigorously through a study of the general-relativistic dynamics of binary systems of strongly self-gravitating bodies [25–28]. Recently, the precision of the $\dot{\omega}$-γ-$\dot{P}_b$ test in PSR 1913+16 data has become so good that it became necessary to correct for the small combined effect of galactic acceleration and proper motion on the observable orbital period change [29].

In addition to providing the first experimental evidence for the existence of gravitational radiation, the $\dot{\omega}$-γ-$\dot{P}_b$ test also represents our first probe of the strong-gravitational-field regime, and therefore has some important consequences. For example, Rosen's bimetric theory, which has the same post-Newtonian limit as general relativity, fails the test by several orders of magnitude because of the interplay between strong-field and radiative effects [30, 16]. (As pointed out in Ref. [31], it also fails the test because of weak-field radiative effects.) However, the $\dot{\omega}$-γ-$\dot{P}_b$ test is a mixed test which combines strong-field and radiative effects in an indistinct way, so that one cannot logically conclude, when the test is satisfied, that both the specific strong-field and radiative predictions of general relativity have been independently confirmed. In fact, examples of theoretically well-motivated theories have recently been constructed [32] which have the same post-Newtonian limit as general relativity, and can pass the $\dot{\omega}$-γ-$\dot{P}_b$ test without fine-tuning, while still differing markedly from Einstein's theory because of the strong self-gravity effects in the pulsar and its companion. In extreme cases the three curves defined by $\dot{\omega}$, γ, and $\dot{P}_b$ can still meet within the observational precision, while the effective gravitational constant between the pulsar and its companion differs by as much as 35% from the usual Newtonian value.

The mixed nature of the $\dot{\omega}$-γ-$\dot{P}_b$ test in PSR 1913+16 raises the following question: Is it possible to extract other tests of relativistic gravity from binary pulsar measurements, specifically tests that probe the quasi-stationary, strong-field aspects of the gravitational interaction? The answer to this question is affirmative, at least in principle, as has been shown by several authors considering different aspects of pulsar data. Immediately after the discovery of PSR 1913+16, it was pointed out [33–35] that a spinning binary pulsar should precess because of relativistic gravitational spin-orbit coupling, and that this effect would show up as a slow change of shape of the electromagnetic pulse as recorded on Earth (see Sec. III for a more complete discussion of this effect, and additional references). More recently it has been shown [36–39] that timing observations of binary pulsars can provide several new tests of strong-field gravity. The main objectives of the present paper will be to present a full account of all the strong-field tests potentially present in pulsar data, and of their physical significance in terms of the correct underlying theory of gravity; and to discuss the observational practicability of these new tests, i.e., the measurability of the parameters entering them. The recent discovery of two new "relativistic" binary pulsars with short-period, highly eccentric orbits, namely PSR 2127+11C [40] and PSR 1534+12 [41], and the fact that additional searches for such objects are underway, makes it timely to discuss the prospects for extracting such new strong-field tests.

Before coming to grips with our specific problem it may be worthwhile to spell out our general views about

the various ways of testing physical theories. First, it seems clear that it is very useful to have a framework which encompasses more than one specific theory. Even in the early days of the confrontation between relativistic gravity and experiment, it was fruitful to compare and contrast general relativity with previous gravitation theories—especially the nonrelativistic theory of Newton, but also, for instance, the relativistic scalar theory of Nordström. Starting in the late 1960s, the utility of having wide classes of alternative theories was made clear by the theoretical discovery of several new post-Newtonian effects that are absent in general relativity, and had therefore been generally overlooked, but are present in alternative theories [5–8]. In some instances what helped in uncovering new effects was the contrast between general relativity and a specific class of theories, in particular the theoretically well-motivated Jordan-Fierz-Brans-Dicke tensor-scalar theory. In other cases it was the existence of a general phenomenological approach to weak-field gravity, the PPN formalism. In the present study we have again found useful both types of approaches: a phenomenological approach to the analysis of pulsar timing data that we shall call, following Ref. [37], the parametrized post-Keplerian (PPK) formalism; and a theory-dependent approach which will contrast general relativity with a specific class of tensor-biscalar theories.

The plan of our paper is as follows. We expose the PPK formalism in full generality in Sec. II, and the potential theoretical significance of its phenomenological parameters in Sec. III. Section IV discusses the present and foreseeable measurability of the PK parameters, primarily by means of numerical simulations based on observational experience with PSR's 1913+16 and 1534+12 [22, 41]. In Sec. V we shift to a theory-dependent approach and show how a fit of timing data to a two-parameter class of tensor-biscalar theories, say $T(\beta', \beta'')$, can constrain the values of the parameters β' and β'' [defined so that $T(0,0)$ reduces to Einstein's theory]. Section VI summarizes our conclusions and the observational prospects for getting new tests of strong-field gravity. Finally, for convenience of the reader we have included an appendix which gathers together the most important symbolic notation, especially those which might lead to confusion. Explicit applications of our methods to real observations of PSR's 1913+16 and 1534+12 have already been carried out, and will be published separately [42].

II. THE PARAMETRIZED POST-KEPLERIAN FORMALISM

A. Phenomenological analysis of timing data

Soon after the discovery of PSR 1913+16, Blandford and Teukolsky [43] derived a timing model, to be fitted to a sequence of pulse arrival times on Earth, which assumed that the pulsar and its companion obeyed the Keplerian kinematical laws. At this level the "Keplerian parameters" entering the timing model are the orbital period P_b, the epoch of periastron passage T_0, the eccentricity e, the longitude of periastron ω, and the projected semimajor axis of the pulsar orbit (in time units), $x \equiv a_1 \sin i/c$ (where a_1 is the semimajor axis of the pulsar orbit, and i the inclination between the orbital plane and the plane of the sky). They completed their model by incorporating the largest short-period relativistic effect, a combination of gravitational redshift and special-relativistic time dilation, quantified by one extra parameter called γ, and by allowing for secular drifts of the main orbital parameters: $P_b = P_{b0} + \dot{P}_b(t-t_0)$, $e = e_0 + \dot{e}(t-t_0)$, $\omega = \omega_0 + \dot{\omega}(t-t_0)$, and $x = x_0 + \dot{x}(t-t_0)$. Although Blandford and Teukolsky (BT) had in mind only to describe within some approximation the general-relativistic dynamics of a two body system, later work [16, 44] showed that the "BT" model was equally able to describe the timing data in a very wide class of alternative relativistic gravity theories. What changes, when the theory changes, are the mathematical expressions linking the phenomenological parameters of the BT model (notably P_b, e, x, $\dot{\omega}$, γ, and $\dot{P}_b$) to the inertial masses of the two neutron stars ($m_1 = m_{\rm pulsar}$, $m_2 = m_{\rm companion}$). As discussed in the Introduction, this fact made it possible, by combining the measurements of the Keplerian parameters P_b, e, x, and the three post-Keplerian parameters $\dot{\omega}$, γ, and $\dot{P}_b$, to get one deep test of a large class of alternative gravity theories.

The situation changed when Epstein [45], and later Haugan [46], set themselves to complete the BT model by deriving, within general relativity, the $O(v^2/c^2)$ fractional contributions to the timing formula arising both from the relativistic "Shapiro time delay" in the gravitational potential of the companion, and from $O(v^2/c^2)$ relativistic post-Keplerian effects in the orbital motion. Their model departed from the attractive phenomenological approach of BT in two ways. First, it was derived within a specific theory of gravity (Einstein's theory), and second, it was so intricate that there seemed to be no clear way of parametrizing the various effects it contained. This led Epstein to abandon the theory-independent features of the BT model and to propose correlating by force all the independent $O(v^2/c^2)$ timing effects by using explicitly the general relativistic expressions linking γ to the masses and the Keplerian parameters. The resulting model has been used to show [21, 22] that the timing data of PSR 1913+16 were accurate enough to require including relativistic effects not part of the original BT model. But the physical significance of these observational findings is unclear, even within the point of view of the Epstein–Haugan model.

Damour and Deruelle [36, 47] proved that it is possible to describe all of the independent $O(v^2/c^2)$ timing effects in a simple mathematical way common to a wide class of alternative theories. This made it possible to revert to a theory-independent analysis of timing data, and led to the possibility of working within a strong-field analogue of the PPN formalism, the so-called [37] "parametrized post-Keplerian" approach. The part of the Damour–Deruelle (DD) phenomenological timing model describing orbital effects reads

$$t_b - t_0 = F[T; \{p^{\rm K}\}; \{p^{\rm PK}\}; \{q^{\rm PK}\}] \,, \tag{2.1a}$$

where t_b denotes the solar-system barycentric (infinite-

frequency) arrival time, T the pulsar proper time (corrected for aberration; see below),

$$\{p^{\rm K}\} = \{P_b, T_0, e_0, \omega_0, x_0\} \tag{2.1b}$$

is the set of Keplerian parameters,

$$\{p^{\rm PK}\} = \{k, \gamma, \dot{P}_b, r, s, \delta_\theta, \dot{e}, \dot{x}\} \tag{2.1c}$$

the set of *separately measurable* post-Keplerian parameters, and

$$\{q^{\rm PK}\} = \{\delta_r, A, B, D\} \tag{2.1d}$$

the set of *not separately measurable* post-Keplerian parameters. The right-hand side of Eq. (2.1a) is given by

$$F(T) = D^{-1}[T + \Delta_R(T) + \Delta_E(T) + \Delta_S(T) + \Delta_A(T)] , \tag{2.2a}$$

$$\Delta_R = x \sin\omega[\cos u - e(1+\delta_r)] + x[1 - e^2(1+\delta_\theta)^2]^{1/2} \cos\omega \sin u , \tag{2.2b}$$

$$\Delta_E = \gamma \sin u , \tag{2.2c}$$

$$\Delta_S = -2r \ln\{1 - e\cos u - s[\sin\omega(\cos u - e) + (1-e^2)^{1/2}\cos\omega \sin u]\}, \tag{2.2d}$$

$$\Delta_A = A\{\sin[\omega + A_e(u)] + e\sin\omega\} + B\{\cos[\omega + A_e(u)] + e\cos\omega\} , \tag{2.2e}$$

where

$$x = x_0 + \dot{x}(T - T_0) , \tag{2.3a}$$

$$e = e_0 + \dot{e}(T - T_0) , \tag{2.3b}$$

and where $A_e(u)$ and ω are the functions of u,

$$A_e(u) = 2\arctan\left[\left(\frac{1+e}{1-e}\right)^{1/2} \tan\frac{u}{2}\right] , \tag{2.3c}$$

$$\omega = \omega_0 + k\, A_e(u) , \tag{2.3d}$$

and u is the function of T defined by solving the Kepler equation

$$u - e\sin u = 2\pi\left[\left(\frac{T - T_0}{P_b}\right) - \frac{1}{2}\dot{P}_b\left(\frac{T - T_0}{P_b}\right)^2\right] . \tag{2.3e}$$

Note that P_b is by definition a constant (the orbital period at epoch T_0), and that the factor $(-1/2)$ in the last term of Eq. (2.3e) comes from integrating the instantaneous orbital frequency $[P_b + \dot{P}_b(T - T_0)]^{-1}$ to obtain the orbital phase. We call attention also to the fact that Eqs. (2.2) and (2.3) represent the "direct timing formula" $t_b = F(T)$ derived in Sec. 2.6 of Ref. [36]. In actual practice, when analyzing binary pulsar data one uses the "inverse timing formula" $T = G(t_b)$ in which solar-system barycentric time is the independent variable (see Sec. 2.7 of Ref. [36] and Sec. IV A below).

The DD model reduces to the BT one after setting $\delta_r = \delta_\theta = r = A = B = 0$, $D = 1$, and replacing $\omega_{\rm DD}(T)$, defined by Eqs. (2.3c)–(2.3e), by the simple linear function $\omega_{\rm BT} = \omega_0 + \dot{\omega}(T - T_0)$. After these replacements the DD parameter k can be simply identified with the BT parameter $\dot{\omega}P_b/2\pi$. More complete descriptions of the DD timing model are given in Refs. [22, 36].

Although the splitting of $F(T)$ into the various contributions (2.2b)–(2.2e) is a coordinate-dependent concept, it is convenient to refer to Δ_R, the time of flight across the orbit, as the "Roemer time delay," to Δ_E as the "Einstein time delay," to Δ_S as the "Shapiro time delay," and to Δ_A as the "aberration delay," or difference between the actual proper time of emission and the corresponding time if the pulsar mechanism had been, say, a radial pulsation instead of a rotating beacon. In this language δ_r and δ_θ quantify relativistic $[O(v^2/c^2)]$ deformations of the orbit, k describes both the secular precession and the short-period "nutation" of the argument of the periastron, r and $s \equiv \sin i$ measure the "range" and "shape" of the Shapiro delay, and A and B parametrize the effects of aberration on pulse timing. For a brief summary of our notation, see also the Appendix below.

As shown in Ref. [36], parameters in the set (2.1d) cannot be measured separately from those in the sets (2.1b), (2.1c) because they can be completely absorbed into suitable redefinitions of the other parameters. The parameter D, a Doppler factor characterizing the center-of-mass motion of the binary pulsar system with respect to the solar-system barycenter (see Eq. (5) of Ref. [36]), can be absorbed in a rescaling of the units of time, length and mass by a factor D. More explicitly, if the observed values of the parameters (2.1b), (2.1c) have been determined by assuming $D = 1$ during the fitting process, they are related to the intrinsic values by

$$P_b^{\rm obs} = D^{-1} P_b^{\rm intrinsic} , \tag{2.4a}$$

$$x^{\rm obs} = D^{-1} x^{\rm intrinsic} , \tag{2.4b}$$

$$e^{\rm obs} = e^{\rm intrinsic} , \text{ etc.} \tag{2.4c}$$

If D were exactly constant in time, the renormalizations (2.4) would drop completely out of any test of gravity theories involving only G and c as dimensioned constants [36]. However, if D has a secular drift, it will induce apparent changes in all of the dimensioned observables, notably in $P_b^{\rm obs}$ and $x^{\rm obs}$. And, indeed, for PSR 1913+16 it has been shown recently [29] that both proper motion of the pulsar and accelerations of the solar system and binary pulsar system in the Galactic gravitational field contribute measurably to a secular drift of $D = 1 - \mathbf{n}\cdot(\mathbf{v}_{\rm solar} - \mathbf{v}_{\rm pulsar})/c + O(v^2/c^2)$, and hence to a secular change of the observed orbital period beyond any intrinsic changes. The corresponding apparent changes in the other timing parameters, notably x, Eq. (2.4b), turn out to be negligible.

The aberration parameters A and B can be absorbed exactly into redefinitions of T_0, x, e, δ_r and δ_θ (see Sec. 3.2 of Ref. [36]). In particular, we have [in addition to the renormalizations (2.4)]

$$x^{\rm obs} = (1 + \varepsilon_A) x^{\rm intrinsic} , \tag{2.5a}$$

$$e^{\rm obs} = (1 + \varepsilon_A) e^{\rm intrinsic} , \tag{2.5b}$$

$$\delta_\theta^{\rm obs} = \delta_\theta^{\rm intrinsic} - \varepsilon_A , \tag{2.5c}$$

$$\delta_r^{\rm obs} = \delta_r^{\rm intrinsic} - 3\varepsilon_A , \tag{2.5d}$$

where

$$\varepsilon_A \equiv \frac{A}{x} = -\frac{P_p}{P_b}\frac{1}{\sin i(1-e^2)^{1/2}}\frac{\sin\eta}{\sin\lambda}\,. \tag{2.6}$$

In Eq. (2.6), derived from the expression given below for A, the quantity P_p denotes the spin period of the pulsar, while λ and η are the polar angles of the spin axis, as defined below. The most interesting physical effects associated with the aberration-induced changes (2.5), (2.6) are the apparent secular changes of $x^{\rm obs}$ and $e^{\rm obs}$ associated with spin-orbit precession of the pulsar spin axis. Let us finally mention that, as discussed in Sec. 3.7 of Ref. [36], δ_r can be reabsorbed in a change of the spin phase of the pulsar, thereby inducing small changes in the observed values of the pulsar rotational parameters which need not concern us here.

Summarizing the results up to now, we see that by fitting the arrival times of a binary pulsar to the DD model (2.1)–(2.3), in which one sets the parameters (2.1d) to some fiducial values $\{\delta_r^{\rm fid}, A^{\rm fid}, B^{\rm fid}, D^{\rm fid}\equiv 1\}$, one can, in principle, measure the Keplerian parameters (2.1b) and eight post-Keplerian parameters (2.1c). The important point is that the eight PK parameters can be measured in a phenomenological manner, independently of the choice of a specific theory of gravity. Within the framework of any relativistic theory, each of the eight PK parameters will be expressible as a theory-dependent function of the dynamical Keplerian parameters P_b, e_0, and x_0, the two unknown inertial masses, m_1 and m_2, and in some cases the polar angles λ and η. (The problems posed by the latter dependence will be treated below, after discussion of the pulse-structure parameters.) In alternative theories one will also have to assume an equation of state for the neutron-star matter. Such an assumption is unnecessary for most of the parameters in general relativity, because of its effacement properties [27]. One expects that, in different theories of gravity, the functions

$$p_i^{\rm PK} = f_i^{\rm theory}(m_1, m_2\,;\, P_b, e_0, x_0\,;\,\text{equation of state}) \tag{2.7}$$

will differ markedly because of the strong-field effects linked with the pulsar and its companion (recall that $Gm/c^2R \simeq 0.2$ for a $1.4\,M_\odot$ neutron star). In Sec. III B we present explicit formulas allowing one to compute the functions $f_i^{\rm theory}$ in a wide class of theories. We also treat in detail in Sec. V A a family of alternative theories in which one can explicitly see the strong-field effects at work.

Our discussion has made it clear that measurement of the Keplerian plus n post-Keplerian parameters will determine n curves in the two-dimensional mass plane whose shape and position depend strongly on the theory of gravity being used. If the theory is "correct" (and if the binary system is "clean," i.e., accurately represented by a simple theoretical model), the n curves should all meet at one point. Thus, the measurement of n post-Keplerian timing parameters yields $n-2$ tests of relativistic gravity, and, more generally, of the other ingredients of the theoretical model of the system. We therefore conclude that in the most favorable circumstances, binary pulsar timing data can provide up to $8-2=6$ tests of relativistic gravity.

Note that to get a useful test one needs to combine the measurement of at least three PK parameters, and that each such test will probe indiscriminately all theoretical effects determining their values. For PSR 1913+16 it has been possible to measure only three PK parameters in such a phenomenological way, namely, $\dot\omega \equiv 2\pi k/P_b$, γ, and $\dot P_b$. These measurements yield, as emphasized in the Introduction, one combined radiative ($\dot P_b$) plus strong-field ($\dot\omega, \gamma$) test of relativistic gravity. The mixed nature of the test makes it very desirable to measure additional PK parameters, in order to probe strong-field effects independently of radiative effects. Before describing the theoretical significance of these extra tests in more detail, we now turn our attention to the information extractable from pulse shape and polarization data.

B. Phenomenological analysis of pulse structure

The structure of pulsar signals (intensity, pulse shape, linear polarization, ...) and its variation with time provides a wealth of information about physical conditions in pulsar magnetospheres and the nature of the radio emission mechanism. For binary pulsars, pulse-structure data can also contain information about gravitational physics, because of interplays between the orbital motion and the gyroscopic nature of the observed periodicity. In the latter category one example that was recognized rather early was the possibility of detecting, through a secular change of pulse shape, the relativistic precession of the spin axis of PSR 1913+16 because of spin-orbit coupling [33, 34, 48]. Another source of potentially measurable effects on pulse structure is the aberration caused by orbital motion of the pulsar, which offers the possibility of measuring several otherwise inaccessible parameters [49, 36]. In the present section we shall generalize previous work on these topics and attempt to specify all the gravitational information potentially available through a careful monitoring of pulse-structure data.

We assumed in Sec. II A that the observed periodic modulation of pulsar signals is caused by rotation of a neutron star about some axis. This assumption made it possible to represent the effects of orbital motion on timing data in a manner independent of any specific emission model. Mathematically, the assumption amounts to linking the pulsar proper time T, used in Eqs. (2.1)–(2.3) to parametrize the orbital effects, to the rotational "phase" of the pulsar, the angle ϕ describing the direction in longitude of the emitted beam, according to the equation

$$\phi(T)/2\pi = \nu_p T + \frac{1}{2}\dot\nu_p T^2 + \frac{1}{6}\ddot\nu_p T^3\,, \tag{2.8}$$

where $\nu_p = 1/P_p$. Actually there is only one place in the timing model (2.1)–(2.3) that requires the assumption that ϕ measures a physical rotation of the pulsar around an axis (rather than, say, the phase of a spherically symmetric pulsation). This is in the addition of the "aberration" timing contribution Δ_A, Eq. (2.2e) (see

Ref. [36]).

On the other hand, when it comes to discussing the effects of the orbital motion on the pulse-structure data, one needs to specify at least some general features of the radio emission. The orbital motion of the pulsar around the center of mass of the binary system produces three different effects: it modulates the flux density received at each frequency by a fixed observer, it Doppler shifts the frequency, and it causes the observer to receive light from a direction, say $\mathbf{n}$, which differs because of aberration from the direction, say $\mathbf{N}$, in which it was emitted in the pulsar comoving frame. If B denotes the blueshift factor experienced by the light, $B \equiv \nu_{\rm obs}/\nu_{\rm emitted}$, the three effects are summarized in the equation

$$\ell(\nu_{\rm obs}, \mathbf{n}, T) = B^3 L(\nu_{\rm emitted}, \mathbf{N}, T) , \tag{2.9}$$

where ℓ denotes the directional spectral luminosity $[d(\text{energy})/d(\text{time})d(\text{frequency})d(\text{solid angle})]$, in the observer's frame, of radiation emitted at the pulsar proper time T, and L denotes the same quantity in the pulsar comoving frame. For our purpose it is sufficient to work to first order in v/c, so that

$$B = \frac{\nu_{\rm obs}}{\nu_{\rm emitted}} = 1 + \mathbf{n}\cdot\boldsymbol{\beta} + O(\beta^2) , \tag{2.10a}$$

$$\mathbf{N} = [1 + (\mathbf{n}\cdot\boldsymbol{\beta})]\mathbf{n} - \boldsymbol{\beta} + O(\beta^2) , \tag{2.10b}$$

where $\boldsymbol{\beta} \equiv \mathbf{v}_1/c$, $\mathbf{v}_1$ denoting the velocity of the pulsar with respect the center of mass of the binary system [50].

At this point, let us state precisely our conventions for the various directional quantities entering the analysis of binary pulsar systems (see Fig. 1). The instantaneous position and orientation of the plane of the orbit with respect to a reference right-handed triad $(\mathbf{I}_0, \mathbf{J}_0, \mathbf{K}_0)$ (denoted $(\mathbf{e}_{X_0}, \mathbf{e}_{Y_0}, \mathbf{e}_{Z_0})$ in Ref. [36]), where

$$\mathbf{K}_0 = -\mathbf{n} \tag{2.11}$$

is the direction from the Earth to the pulsar and $(\mathbf{I}_0, \mathbf{J}_0)$ are reference directions in the plane of the sky, is defined by two angles: the longitude of the ascending node Ω $(0 \leq \Omega < 2\pi)$ and the inclination i $(0 \leq i < \pi)$. More precisely, one passes from the reference triad $(\mathbf{I}_0, \mathbf{J}_0, \mathbf{K}_0)$ to an "orbital" (right-handed) triad $(\mathbf{i}, \mathbf{j}, \mathbf{k})$ (denoted $(\mathbf{e}_x, \mathbf{e}_y, \mathbf{e}_z)$ in Ref. [36]) by two successive rotations: first, a rotation of Ω around $\mathbf{K}_0$ which yields

$$\mathbf{I} = \cos\Omega\mathbf{I}_0 + \sin\Omega\mathbf{J}_0 , \tag{2.12a}$$

$$\mathbf{J} = -\sin\Omega\mathbf{I}_0 + \cos\Omega\mathbf{J}_0 , \tag{2.12b}$$

$$\mathbf{K} = \mathbf{K}_0 , \tag{2.12c}$$

and second, a rotation of i around the direction of the ascending node $\mathbf{I} = \mathbf{i}$,

$$\mathbf{i} = \mathbf{I} , \tag{2.13a}$$

$$\mathbf{j} = \cos i\mathbf{J} + \sin i\mathbf{K} , \tag{2.13b}$$

$$\mathbf{k} = -\sin i\mathbf{J} + \cos i\mathbf{K} . \tag{2.13c}$$

The orbital motion takes place in the plane $(\mathbf{i}, \mathbf{j})$, which intersects the plane of the sky along the direction of the ascending node $\mathbf{I} = \mathbf{i}$, and is oriented in the positive direction (so that $\mathbf{k} = \mathbf{i} \times \mathbf{j}$ is the unit vector in the direction of the orbital angular momentum). For simplicity we define

$$C(u) \equiv \cos[\omega + A_e(u)] + e\cos\omega , \tag{2.14a}$$

$$S(u) \equiv \sin[\omega + A_e(u)] + e\sin\omega , \tag{2.14b}$$

$$\beta_1 \equiv n\, x(1-e^2)^{-1/2} , \tag{2.14c}$$

where $n \equiv 2\pi/P_b$ is the orbital mean motion and $x \equiv a_1 \sin i/c$ the Keplerian timing parameter (projected semimajor axis) introduced above. The orbital velocity of the pulsar is then given, to first order, by

$$\boldsymbol{\beta} \equiv \frac{\mathbf{v}_1}{c} = \frac{\beta_1}{\sin i}[-S(u)\,\mathbf{i} + C(u)\,\mathbf{j}] . \tag{2.15}$$

For any emission model of the pulsar, i.e., any specific form of the comoving luminosity $L(\nu, \mathbf{N}, T)$, the formulas (2.9)–(2.15) specify explicitly the influence of orbital motion on the flux density $[d(\text{energy})/d(\text{time})d(\text{frequency})d(\text{area})]$ observable at the solar-system barycenter, $S(\nu_{\rm obs}) = \ell(\nu_{\rm obs}, \mathbf{n})/d^2$, where d is the distance between the barycenter and the pulsar. To give an example of the information obtainable from the interplay between orbital motion and pulse-structure data, let us consider the rotating magnetic pole model [51]. In this model, which is supported by many pulsar observations, see, e.g., Ref. [52], both the intensity and polarization features of pulsar emission can be described in simple geometrical terms by considering the emission to be due to curvature radiation along the field lines of a dipolar magnetic field rotating rigidly in space. This means, in the simplest version of the model, that the directional luminosity in the proper pulsar frame is a function only of the angle between the emission direction $\mathbf{N}$ and a rotating unit vector $\mathbf{b}(T)$ pointing along the magnetic axis, while the radiation is polarized (at emission) along the vector tangent, at $\mathbf{N}$, to the great circle joining $\mathbf{N}$ to $\mathbf{b}(T)$ on the sphere of unit vectors (see Fig. 10-4 of Ref. [52]). An explicit expression of the effects of aberration on pulse intensity in this model can then be obtained by combining Eqs. (2.9)–(2.15) with the usual expressions for the rotating vector model [52]. It reads

$$S_{\rm obs}(\nu_{\rm obs}, T) = (1+3\mathbf{n}\cdot\boldsymbol{\beta})\, F_p[(1-\mathbf{n}\cdot\boldsymbol{\beta})\nu_{\rm obs}, \mathbf{N}\cdot\mathbf{b}(T)] , \tag{2.16}$$

where

$$\mathbf{n}\cdot\boldsymbol{\beta} = -\beta_1 C(u) , \tag{2.17}$$

$$\mathbf{N}\cdot\mathbf{b}(T) = \cos\alpha\cos\zeta_\beta + \sin\alpha\sin\zeta_\beta\cos(\phi - \phi_0) , \tag{2.18}$$

$$\zeta_\beta = \zeta + \delta_{\rm A}\zeta , \tag{2.19}$$

$$\delta_{\rm A}\zeta = \frac{\beta_1}{\sin i}[-\cos\eta S(u) + \cos i\sin\eta C(u)] . \tag{2.20}$$

Let ψ denote the linear polarization angle, defined modulo π and measured positively in the clockwise direction in the plane of the sky, as seen from the Earth. [Beware that this sign convention is opposite to the usual observers' practice; it is dictated by the sense of orientation induced in the plane $(\mathbf{I}_0, \mathbf{J}_0)$ by righthandedness of the triad $(\mathbf{I}_0, \mathbf{J}_0, \mathbf{K}_0)$, which is counterclockwise when

seen from "above," but clockwise when seen from below, i.e., by the observer; see Fig. 1(a).] The variation of ψ with pulsar phase is given by

$$\tan[\psi(\phi)-\psi_{0\beta}] = \frac{\sin\alpha\,\sin(\phi-\phi_0)}{\cos\alpha\,\sin\zeta_\beta - \sin\alpha\,\cos\zeta_\beta\cos(\phi-\phi_0)}\ , \tag{2.21}$$

$$\psi_{0\beta} = \psi_0 + \delta_{\rm A}\psi_0\ , \tag{2.22}$$

$$\psi_0 = \Omega + \eta + \psi_{\rm Faraday}\ , \tag{2.23}$$

$$\delta_{\rm A}\psi_0 = -\beta_1 \frac{\cot\lambda}{\sin i}\,[\sin\eta S(u) + \cos i\cos\eta C(u)]\ . \tag{2.24}$$

In Eqs. (2.16)–(2.24) $F_p(\nu,\cos\theta)$ is a fixed function giving the intrinsic luminosity of the pulsar, in its proper frame, at frequency ν and in a direction making an angle θ with the instantaneous magnetic axis, while α is the fixed angle ($0 \le \alpha < \pi$) between the pulsar spin axis, say $\mathbf{s}_1 = \mathbf{S}_1/|\mathbf{S}_1|$, and the rotating magnetic axis $\mathbf{b}(T)$ [oriented so as to be closest to the direction of the observer at the time of emission of the main pulse, see Fig. 1(b)], so that $\cos\alpha = \mathbf{s}_1\cdot\mathbf{b}(T)$. The direction of $\mathbf{s}_1$ with respect to the triad $(\mathbf{I},\mathbf{J},\mathbf{K})$ of Eqs. (2.12) is coded in the two polar angles (λ,η), or equivalently (ζ,η) (with $0 \le \lambda < \pi$, $0 \le \zeta < \pi$, $0 \le \eta < 2\pi$), such that

$$\mathbf{s}_1 = \sin\lambda\,\cos\eta\,\mathbf{I} + \sin\lambda\,\sin\eta\,\mathbf{J} + \cos\lambda\,\mathbf{K}\ , \tag{2.25a}$$

$$\zeta \equiv \pi - \lambda\ . \tag{2.25b}$$

It is useful to keep in mind that in the case of perfect parallel (rather than antiparallel) alignment of spin and orbital angular momenta, i.e. $\mathbf{s}_1 = +\mathbf{k}$ (where the plus sign has its physical origin in the fact that the observed pulsar is thought to have been spun up by the orbital angular momentum), the two polar angles become, without ambiguity, $\lambda = i$ and $\eta = -\pi/2$. *A priori*, we expect real situations to differ only by a small or moderate amount from this aligned case [see Eqs. (3.36) and end of Sec IV D for further discussion of "misaligned" cases].

The angles λ and η, with λ being the angle between $\mathbf{s}_1$ and $\mathbf{K} = \mathbf{K}_0$, appear naturally in the analysis of timing data, while the supplementary angle ζ appears naturally in the analysis of pulse structure data as the angle between $\mathbf{s}_1$ and the direction from the pulsar to the Earth, $\mathbf{n} = -\mathbf{K}$ (see Fig 1). The orbital-phase-dependent angle ζ_β appearing in Eq. (2.18) is the angle between $\mathbf{s}_1$ and the instantaneous observer's direction $\mathbf{N}$, as seen in the pulsar frame. The direction $\mathbf{n}$ is viewed in the center-of-mass frame and is fixed, while $\mathbf{N}$ undergoes periodic changes because of aberration [see Eq. (2.10b)]. Hence, the angle ζ_β varies during one orbital period by an amount given by Eq. (2.20), while ζ (or λ) and η vary only over the much longer time scale of variation of $\mathbf{s}_1$ with respect to a locally inertial frame attached to the center of mass of the binary system ("spin-orbit" precession, see Sec. III). The direction $\mathbf{N}$ varies because of aberration both in latitude ($\delta_{\rm A}\zeta$) and in longitude ($\delta_{\rm A}\phi_0$). However, the longitude change is equivalent to a change in the phase of the pulsar, and has already been incorporated in the observable phase ϕ by including the aberration term Δ_A in the timing model (2.1)–(2.3) (see Sec. 2.4 of Ref. [36]). As a consequence, the angle ϕ_0 in Eqs. (2.18) and (2.21) is just a constant offset.

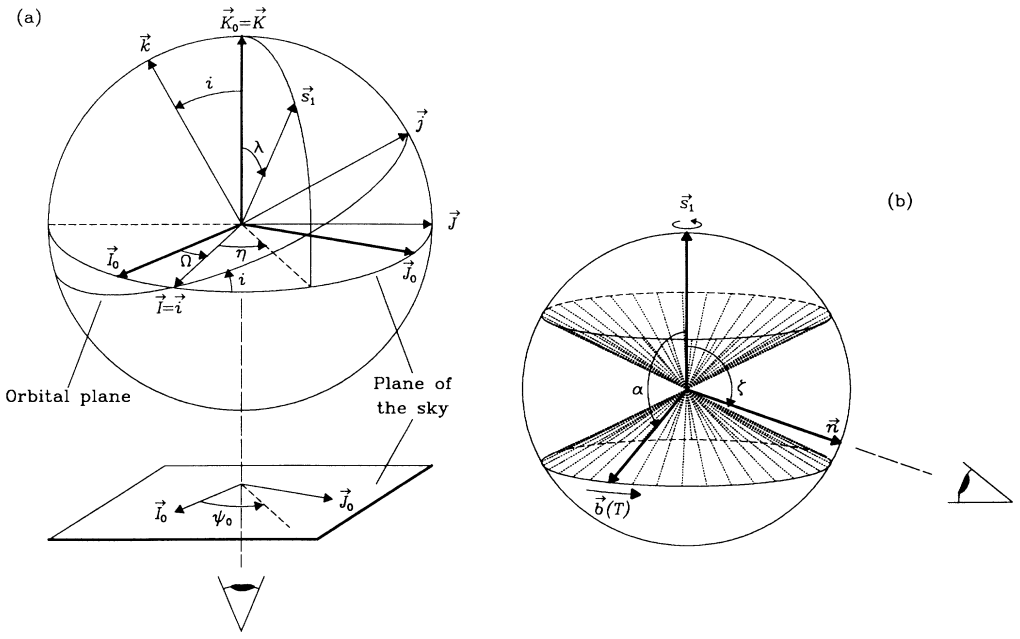

FIG. 1. Angles and orientation conventions relating both the orbit (a) and the spinning pulsar (b) to the observer's coordinate system and the line of sight. The orbital plane is inclined at angle i with respect to the plane of the sky; directions of the pulsar's spin and orbital angular momenta and its magnetic axis are $\mathbf{s}_1$, $\mathbf{k}$, and $\mathbf{b}(T)$, respectively. (Vectors are denoted with boldface in the text, but with overarrows in this figure.) See text for definitions of other angles.

The orbital-phase-dependent polarization offset $\psi_{0\beta}$ appearing in Eq. (2.21) results from applying the boost β (and the effect of the interstellar medium) onto the direction, as seen in the pulsar frame, of the electric vector of the signal emitted at the center of the main pulse: $\mathbf{E} \propto \mathbf{s}_1 - \mathbf{N}(\mathbf{N}\cdot\mathbf{s}_1)$. Hence, the angle $\psi_{0\beta}$ changes, like ζ_β, on an orbital time scale because of the aberration contribution (2.24), as well as on the much longer time scale of variation of $\mathbf{s}_1$. In Eq. (2.23) Ω denotes the longitude of the ascending node, as defined in Eqs. (2.12); it provides one of the necessary links between the orbit-based coordinate system and the observer's system [see Fig 1(a)]. The last term in (2.23) represents the effect of Faraday rotation along the path of signal propagation, which must be measured and subtracted in order to gain access to the interesting information contained in the other causes of variation of $\psi_{0\beta}$.

By analogy with the discussion in Sec. II A concerning timing data, the main question we wish to address here is: How many new parameters can, in principle, be extracted from pulse-structure data? Let us first emphasize that all formulas used in the present subsection are independent of the choice of a specific relativistic theory of gravity. They depend only on special-relativistic effects and on the lowest-order Keplerian kinematics of a binary system. However, they do depend on the choice of the rotating-pole model of pulsar emission, and this model dependence should be kept in mind if tests issuing from pulse-structure parameters are ever found to conflict with tests issuing from timing parameters.

Because the time-dependent blueshift factor $B = 1 + \mathbf{n}\cdot\boldsymbol{\beta} + O(\beta^2)$ is known from the Keplerian-level timing data, all its effects in Eq. (2.16) can be computed rather than fitted for. This leaves the following new set of parameters available from pulse-structure data, thanks to the interplay of spin and orbital effects: α, ζ, $\cos\eta/\sin i$, $\cot i \sin\eta$, $\cot\lambda\ \cot i\cos\eta$, $\cot\lambda \sin\eta/\sin i$, ψ_0, and ϕ_0. Monitoring of the pulse shape and polarization over several years can also give access to secular drifts of these parameters (as expected for ζ and η because of spin-orbit precession of the pulsar axis). Among these parameters, three contain no gravitational information: ϕ_0 and ψ_0 depend on arbitrary choices of origins for angles, and α, although astrophysically interesting, is not coupled to the binary system dynamics. Finally, under the assumptions of the rotating magnetic pole model, we have the following new set of "post-Keplerian" parameters, extractable in principle from pulse-structure data:

$$\{\tilde{p}^{\mathrm{PK}}\} = \{\lambda, \dot{\lambda}, \kappa, \dot{\kappa}, \sigma, \dot{\sigma}, \dot{\psi}_0, \kappa', \dot{\kappa}', \sigma', \dot{\sigma}'\} , \qquad (2.26)$$

where we have used $\lambda \equiv \pi - \zeta$ ($\cos\lambda = \mathbf{s}_1\cdot\mathbf{K}$) instead of ζ ($\cos\zeta = \mathbf{s}_1\cdot\mathbf{n}$), and we have introduced the notation

$$\kappa \equiv (\sin i)^{-1}\cos\eta , \qquad (2.27a)$$

$$\sigma \equiv \cot i \sin\eta , \qquad (2.27b)$$

$$\kappa' \equiv \cot\lambda \cot i \cos\eta , \qquad (2.28a)$$

$$\sigma' \equiv \cot\lambda (\sin i)^{-1} \sin\eta , \qquad (2.28b)$$

for the parameters appearing directly in the measurable effects. We note in passing that even in cases where $\sin i$ is known from the timing data, $\cos i$ is determined only up to a sign, so that the simultaneous measurement of, e.g., $s \equiv \sin i$, κ, and σ determines i and η only modulo the residual ambiguity $i \to \pi - i$, $\eta \to -\eta$.

III. THEORETICAL CONTENT OF POST-KEPLERIAN PARAMETERS

In the previous section we have shown that one can, in principle, extract two sets of post-Keplerian parameters from pulsar data in a theory-independent way: 8 "timing" parameters (2.1c), and 11 "pulse-structure" ones (2.26). In order to exhibit the theoretical importance of measuring these parameters, in particular for providing tests of the strong-field aspects of relativistic gravity, we shall use the framework of a very general class of relativistic gravity theories. Then, within such a framework, we shall derive the expressions linking these parameters to the Keplerian ones and to the inertial masses of the pulsar and its companion, i.e., the functions (2.7). (As we shall see explicitly, some of these depend also on the polar angles of the spin axis.) The theory dependence of the functions (2.7) will then allow us to assess the theoretical content of experimental measurements of each phenomenological parameter.

A. A generic class of relativistic gravity theories

Let us consider the class of theories which generalize to the strong-field regime the Eddington β-γ parametrized post-Newtonian metric, i.e., theories in which the effective gravitational interaction between compact bodies is fully conservative and has neither preferred-frame nor preferred-location effects. We shall consider only Lagrangian-based theories, and we take "fully conservative" to mean that the Lagrangian is invariant (modulo a total time derivative) under the Poincaré group. Under these assumptions, Will [16] has shown (see also [53, 54]) that the general form of the Lagrangian describing the orbital dynamics of N compact bodies (with positions $\mathbf{z}_A$ and velocities $\mathbf{v}_A$; $A = 1, \ldots, N$) can be written, when keeping only terms of order $(v/c)^2$ beyond an effective Newtonian interaction, as

$$L_{\mathrm{O}}(\mathbf{z}_A, \mathbf{v}_A) = -\sum_A m_A c^2 \left(1 - \frac{1}{2c^2}\mathbf{v}_A^2 - \frac{1}{8c^4}\mathbf{v}_A^4\right)$$
$$+ \frac{1}{2}\sum_A \sum_{B\neq A} \frac{G_{AB} m_A m_B}{r_{AB}} \left(1 + \frac{1}{2c^2}\varepsilon_{AB}(\mathbf{v}_A^2 + \mathbf{v}_B^2) - \frac{1}{2c^2}(1 + 2\varepsilon_{AB})(\mathbf{v}_A\cdot\mathbf{v}_B)\right.$$
$$\left. - \frac{1}{2c^2}(\mathbf{n}_{AB}\cdot\mathbf{v}_A)(\mathbf{n}_{AB}\cdot\mathbf{v}_B)\right) - \frac{1}{2}\sum_A \sum_{B\neq A} \sum_{C\neq A} \frac{G^A_{BC} m_A m_B m_C}{c^2 r_{AB} r_{AC}} . \qquad (3.1)$$

In this equation $r_{AB} \equiv |\mathbf{z}_A(t) - \mathbf{z}_B(t)|$, $\mathbf{n}_{AB} \equiv (\mathbf{z}_A - \mathbf{z}_B)/r_{AB}$, the m_A's denote the inertial masses of the bodies (including gravitational binding energy), and G_{AB} denotes the effective Newtonian constant for the gravitational interaction between compact bodies labeled A and B. We assume here that strong-field effects associated with the self-gravity of each compact body are treated exactly, but we expand in the small parameter $(v^{\rm orbit}/c)^2 \sim G_{AB}m_A/r_{AB}c^2$ which characterizes the weak relativistic gravitational coupling between two well-separated compact bodies. This means that even at the "Keplerian level," where one keeps only the $G_{AB}m_Am_B/r_{AB}$ interaction between two bodies, the effective gravitational constant G_{AB} will in general differ by strong-field effects from the usual Newtonian constant G. Section V A contains some explicit examples of such effects in tensor-biscalar theories.

Similarly, the quantities in the Lagrangian (3.1) associated with $O(v^2/c^2)$ orbital effects, namely, ε_{AB} (associated with velocity-dependent or "magnetic" effects) and G^A_{BC} (associated with nonlinear relativistic gravitational couplings) will differ by strong-field effects from their values in the weak-field limit, respectively, $\varepsilon_{AB} = 2\gamma+1$ and $G^A_{BC} = (2\beta-1)G^2$, in terms of the usual Eddington parameters β and γ. General relativity differs from generic theories of gravity in that all strong-field effects are "effaced" in relativity: once lumped into the observable inertial masses, self-gravity effects are renormalized away. Explicitly, in general relativity one has $(G_{AB})^{\rm GR} = G$, $(\varepsilon_{AB})^{\rm GR} = 3$, and $(G^A_{BC})^{\rm GR} = G^2$, both for ordinary and compact bodies. We thereby see that any measurable parameter whose interpretation within the framework of Eq. (3.1) depends on either G_{AB}, ε_{AB}, or G^A_{BC} is of potential interest as a test of strong-field gravity.

In order to discuss all potentially observable parameters in binary pulsar systems, we need to complete the orbital Lagrangian (3.1) by adding the general form of relativistic spin-orbit effects. In keeping with the assumptions made above, we shall require invariance under Poincaré transformations and notably under Lorentz boosts. As first discussed explicitly by Damour [26], this implies that the spin-orbit Lagrangian depends not only on positions and velocities but also on accelerations. Actually, the acceleration-dependent piece of the Lagrangian obtained in Ref. [26] is just

$$L^{(T)}_{\rm SO}(\mathbf{z}_A,\mathbf{v}_A,\mathbf{a}_A) = \sum_A \frac{1}{2c^2} S^{ij}_A v^i_A a^j_A \ , \tag{3.2}$$

where $S^{ij}_A \equiv \varepsilon^{ijk}S^k_A$ is the spin vector of body A and $\mathbf{a}_A = d\mathbf{v}_A/dt$ its acceleration. Equation (3.2) is independent of the source of physical interaction between the bodies and is the manifestation, within the Lorentz-invariant Lagrangian formalism, of the famous Thomas precession (which enters all spin-orbit effects, whether linked with electromagnetic or gravitational interactions).

The remaining part of the spin-orbit Lagrangian of Ref. [26] depends on the specific gravity theory chosen (general relativity in that case) and one may expect it to be modified by strong-field effects in generic theories. As this second piece is separately boost invariant, it is easy to generalize it to an arbitrary boost-invariant theory. This leads us to write the following general form of the spin-orbit interaction term within our general class of theories:

$$L_{\rm SO}(\mathbf{z}_A,\mathbf{v}_A,\mathbf{a}_A) = \sum_A \frac{1}{c^2} S^{ij}_A \Bigg(\frac{1}{2} v^i_A a^j_A + \sum_{B\neq A} \frac{\Gamma^B_A m_B}{r^3_{AB}} \times (v^i_A - v^i_B)(z^j_A - z^j_B) \Bigg) \ . \tag{3.3}$$

The possible influence of strong-field effects in spin-orbit phenomena shows up in the appearance of the coupling function Γ^B_A, which is simply equal to $2G$ in general relativity [55, 56, 26], but which is expected to be modified by self-gravity contributions in other theories. One already knows that $\Gamma^B_A = (\gamma+1)G$ in the PPN framework [57], which suggests that in general Γ^B_A may be equal to $\frac{1}{2}(\varepsilon_{AB}+1)G_{AB}$. In absence of a theory of the motion of spinning compact bodies in a generic theory of gravity, we shall keep Γ^B_A as a free strong-field parameter, and assume nothing about its symmetry under exchange of the labels A and B.

The orbital dynamics of a binary pulsar system is obtainable from the total orbital Lagrangian

$$L^{\rm tot}_{\rm O}(\mathbf{z}_A,\mathbf{v}_A,\mathbf{a}_A) = L_{\rm O} + L_{\rm SO} \ , \tag{3.4}$$

in which the spin vectors play the role of given, slowly evolving, external fields (see Sec. III B for a discussion of the effect on the spins of the spin-orbit interaction). As recently pointed out [29, 39], one cannot simply limit the summations in Eqs. (3.1) and (3.3) to the two labels, say 1 and 2, corresponding to the pulsar and its companion, because the influence of the Galaxy can be important enough to lead to measurable effects. However, for simplicity's sake we shall first consider the binary orbital effects by themselves, and later add the (strong-field-modified) Galactic effects. Actually, the work of Ref. [39] shows that, for pulsars of the type we shall consider here, quasiperiodic timing effects linked to violation of the strong equivalence principle [$\Delta \equiv (G_{13} - G_{23})/G \neq 0$, where the label 3 corresponds to the Galaxy] are negligibly small, and their contributions to $\dot{x}$ and $\dot{e}$ are smaller than the effects of gravitational-wave damping (in general relativity) as long as $|\Delta| < 0.18$. The present work and a sequel paper [42] will show that existing timing data already restrict such violations of the strong equivalence principle enough to allow us to neglect such effects in advance. As for the other, more standard, Galactic effects discussed in [29] within the general relativistic context, we will discuss their contribution to $\dot{P}_b$ separately in Sec. III B.

Considering then the Lagrangian (3.4) for an isolated binary system ($A, B = 1, 2$), we can take advantage of its Poincaré invariance to go to the center-of-mass frame of the binary system. Moreover, following the work of Damour and Shäfer [38] we can eliminate the accelerations by means of the coordinate shift $r^i_A = z^i_A + S^{ij}_A v^j_A/(2m_Ac^2)$. Finally we obtain the following Lagrangian for the relative motion ($\mathbf{R} \equiv \mathbf{r}_1 - \mathbf{r}_2$, $\mathbf{V} \equiv$

$\mathbf{v}_1 - \mathbf{v}_2$):

$$L^R(\mathbf{R},\mathbf{V}) = \mu \hat{L}^R_{\rm O} + L'_{\rm SO} \ , \tag{3.5a}$$

$$\hat{L}^R_{\rm O}(\mathbf{R},\mathbf{V}) = \frac{1}{2}\mathbf{V}^2 + \frac{\mathcal{G}M}{R} + \frac{1}{8c^2}(1-3\nu)\mathbf{V}^4 + \frac{\mathcal{G}M}{2Rc^2}\left((\varepsilon+\nu)\mathbf{V}^2 + \nu(\mathbf{N}\cdot\mathbf{V})^2 - \xi\frac{\mathcal{G}M}{R}\right) \ , \tag{3.5b}$$

$$L'_{\rm SO} = -\sum_{A=1}^{2} \sigma_A \mathbf{S}_A \cdot \mathbf{L}/R^3 \ . \tag{3.5c}$$

In Eqs. (3.5) $\mathbf{L}$ denotes the orbital angular momentum in the center-of-mass frame $[\mu\mathbf{R}\times\mathbf{V} + O(c^{-2})]$, $\mathbf{N}$ denotes (here and only here) the unit vector $\mathbf{R}/R$, and the $\mathbf{S}_A$'s are the same spin vectors as used above. We have used the shorthand notation $M \equiv m_1 + m_2$, $\mu \equiv m_1 m_2/M$, $\nu \equiv \mu/M$ (with $0 \le \nu \le 1/4$), $\mathcal{G} \equiv G_{12}$ (effective gravitational constant between the pulsar and its companion), $\varepsilon \equiv \varepsilon_{12}$, and

$$\xi \equiv (m_1 G^2_{11} + m_2 G^1_{22}) M^{-1} \mathcal{G}^{-2} \ , \tag{3.6a}$$

$$\sigma_A \equiv c^{-2}[\Gamma^B_A + (\Gamma^B_A - \tfrac{1}{2}G_{AB})(m_B/m_A)] \ , \quad (A=1,2; B\neq A) \ . \tag{3.6b}$$

The possible differences between a generic theory of gravity and general relativity lie in the quantities $\mathcal{G}$, ε, ξ, σ_1 and σ_2, which in Einstein's theory are, respectively, equal to G, 3, 1, and

$$(\sigma_A)^{\rm GR} = \frac{G}{c^2}\left(2 + \frac{3}{2}\frac{m_B}{m_A}\right) \ . \tag{3.7}$$

B. Post–Keplerian parameters in generic gravity theories

Let us first consider the pure orbital dynamics resulting from the Lagrangian $\hat{L}^R_{\rm O}$, Eq. (3.5b). Following the method of Damour and Deruelle [47], one can write the solution for the relative orbital motion, including $O(v^2/c^2)$ contributions, in a simple quasi-Newtonian form. The influence of strong-field effects in a generic theory appears in modifications of the general relativistic Eqs. (2.17) of Ref. [47] for the coefficients therein called A, B, C, D, H, and I [these denote the coefficients of the various powers of R^{-1} that appear when one expresses $(dR/dt)^2$ and $d\theta/dt$ in terms of R and the relative orbital energy and angular momentum, E and J]. Subsequent relations involving these quantities, and particularly Eqs. (3.3)–(3.5), (4.11), and (4.12) of Ref. [47], which define the post-Newtonian motion in a binary system to order $(v/c)^2$, require no further changes. Moreover, one can show that the only modification in the relativistic center-of-mass integral (associated with the boost invariance of the Lagrangian) is to replace G by $\mathcal{G}$ in Eq. (2.3b) of Ref. [47]. This substitution propagates to Eqs. (2.4) and (6.1)–(6.3) therein, and allows us to get simple expressions for the relativistic motion of the pulsar around the center of mass. We can then follow the method of Ref. [36] to derive the explicit timing formula in a generic gravity theory. The only modifications, brought by a new gravity theory, to the derivation in [36] are (see Ref. [16]) (i) the need to take into account the Keplerian mass (which enters g_{00}) of the companion in the gravitational redshift of the pulsar clock, (ii) the possible addition of a contribution arising from orbital modulation of the pulsar's moment of inertia (written, following Refs. [16,44], as $\Delta I_1/I_1 = +\kappa\eta^* m_2/Rc^2$ where $\kappa \equiv -\partial \ln I_1/\partial \ln G_1^{\rm local}$, and where η^* measures the influence of the proximity of the companion on the value of the gravitational constant at the location of the pulsar, $G_1^{\rm local} = G(1-\eta^* m_2/Rc^2)$), and (iii) the need to take into account both the Keplerian mass (in g_{00}) and the "space curvature" one (in g_{ij}) when computing the Shapiro time delay.

To express conveniently the final results, which replace Eqs. (33)–(37) of Ref. [36] in a generic boost-invariant relativistic gravity, let us introduce the dimensionless variables

$$X_1 \equiv m_1/M \quad \text{and} \quad X_2 \equiv m_2/M \quad (\text{with } X_1 + X_2 \equiv 1,\ X_1 X_2 = \nu) \ , \tag{3.8a}$$

$$\beta_O \equiv (\mathcal{G}Mn/c^3)^{1/3} \ , \tag{3.8b}$$

$$\delta \equiv n\gamma/e \ . \tag{3.8c}$$

Then, using the form taken by Kepler's third law in a generic theory of gravity, namely,

$$a_R = \left(\frac{\mathcal{G}M}{n^2}\right)^{1/3}\left[1 - \frac{1}{6}(5\varepsilon + 3 - 2\nu)\left(\frac{\mathcal{G}Mn}{c^3}\right)^{2/3}\right] \ , \tag{3.9}$$

where a_R denotes the semimajor axis of the relative orbit, we can express the phenomenological parameters of the DD model coming from the $O(v^2/c^2)$-accurate orbital dynamics in terms of the Keplerian parameters ($n \equiv 2\pi/P_b$, x, and e) and of the two masses m_1 and m_2 [see Eq. (2.7)]:

$$k = (\varepsilon - \tfrac{1}{2}\xi + \tfrac{1}{2})\frac{\beta_O^2}{1-e^2} \ , \tag{3.10}$$

$$\delta = X_2\,(G_{02} + X_2\mathcal{G} + \kappa\eta^*)\frac{\beta_O^2}{\mathcal{G}} \ , \tag{3.11}$$

$$\delta_r^{\rm intrinsic} = (\varepsilon + 1 - \nu - X_1^2)\,\beta_O^2 - \delta \ , \tag{3.12}$$

$$\delta_\theta^{\rm intrinsic} = (\varepsilon + 1 - \nu - \tfrac{1}{2}X_1^2)\,\beta_O^2 - \delta \ , \tag{3.13}$$

$$r = \frac{1}{4c^3}G_{02}(1+\varepsilon_{02})m_2 \ , \tag{3.14}$$

$$s = \frac{nx}{\beta_O X_2} \ , \tag{3.15}$$

$$A = -\frac{\beta_O X_2}{2\pi\nu_p(1-e^2)^{1/2}}\frac{\sin\eta}{\sin\lambda} \ , \tag{3.16}$$

$$B = -\frac{\beta_O X_2}{2\pi\nu_p(1-e^2)^{1/2}}\frac{\cos i\cos\eta}{\sin\lambda} \ . \tag{3.17}$$

In these equations $\mathcal{G} \equiv G_{12}$, $\varepsilon \equiv \varepsilon_{12}$, and ξ have been defined above [Eq. (3.6a)]; G_{02} denotes the effective gravitational constant between the (compact) companion m_2 and any noncompact test particle ($m_0 \to 0$); similarly, $\varepsilon_{02} = \varepsilon_{AB}$ for $m_A = m_0 \to 0$, $m_B = m_2$. Note that although the parameter s denotes simply $\sin i$, the elimination of $a_1 \equiv X_2 a_R \equiv cx/\sin i$ in terms of the masses and the orbital period introduces a theory dependence because of Kepler's third law (3.9). We have expressed the aberration parameters (given in any theory by Eqs. (38) and (39) of Ref. [36]) in terms of the masses, the orbital period, and the polar angles of the spin vector introduced in Eq. (2.25a). [However, we left $\cos i$ in Eq. (3.17) without replacing it in terms of $s \equiv \sin i$ because its sign is *a priori* unknown.] Moreover, one should remember from Eqs. (2.5) above that δ_θ given by Eq. (3.13) is the intrinsic value of this parameter, but that when the (unmeasurable) aberration parameter A is replaced by some fiducial value, say A_0, the observed value of δ_θ will be

$$\delta_\theta^{\rm obs} = \delta_\theta^{\rm intrinsic} - (\varepsilon_A - \varepsilon_{A_0}) , \tag{3.18}$$

with $\varepsilon_A \equiv A/x$ and $\varepsilon_{A_0} \equiv A_0/x$.

In addition to the post-Keplerian timing parameters (3.10)–(3.17), linked to the orbital Lagrangian at order $(v/c)^2$ and to aberration effects, there are further timing parameters linked either to spin-orbit effects or to higher-order relativistic effects, notably gravitational-wave damping of the system. Both types will contribute to intrinsic secular changes of the Keplerian parameters; for example, we expect changes in $x \equiv a_1 \sin i/c$ because the orbit shrinks under gravitational-wave damping, and also because the inclination changes via spin-orbit effects. Moreover, as discussed above, if we fix the unmeasurable parameters A, B, and D to some fiducial values, the spin-orbit coupling and the varying Doppler effect between the pulsar system and the solar system will introduce further apparent changes in the observable parameters $P_b^{\rm obs}$, $x^{\rm obs}$, and $e^{\rm obs}$. Finally, we can write

$$\left(\frac{\dot P_b}{P_b}\right)^{\rm obs} = \left(\frac{\dot P_b}{P_b}\right)^{\rm GW} - \frac{\dot D}{D} , \tag{3.19}$$

$$\left(\frac{\dot x}{x}\right)^{\rm obs} = \left(\frac{\dot a_1}{a_1}\right)^{\rm GW} + \left(\cot i \frac{di}{dt}\right)^{\rm SO} + \frac{d\varepsilon_A}{dt} - \frac{\dot D}{D} , \tag{3.20}$$

$$\left(\frac{\dot e}{e}\right)^{\rm obs} = \left(\frac{\dot e}{e}\right)^{\rm GW} + \frac{d\varepsilon_A}{dt} , \tag{3.21}$$

where $\varepsilon_A \equiv A/x$ as above. We shall not attempt here to give precise expressions for the gravitational-wave damping contributions in Eqs. (3.19)–(3.21). Indeed, such high-order, mixed radiative and strong-field effects depend in a complicated way on the structure of a gravity theory and are not as easy to describe in terms of a small number of arbitrary functions as was possible for the PK parameters (3.10)–(3.17). See, however, Ref. [32] for the derivation of $\dot P_b$ in the general class of tensor-multiscalar theories.

The contribution of the varying Doppler shift reads [29]

$$-\frac{\dot D}{D} = \frac{1}{c}\mathbf{K}\cdot(\mathbf{a}_{\rm psr\ system} - \mathbf{a}_{\rm solar\ system}) + \frac{v_T^2}{cd} , \tag{3.22}$$

where the acceleration $\mathbf{a}_{\rm solar\ system}$ is given by the standard Galactic acceleration at the solar location, $\mathbf{g}_{\rm solar}$, but where the acceleration of gravitational free fall of the pulsar system is modified, in a generic gravity theory, to

$$\mathbf{a}_{\rm psr\ system} = G^{-1}(X_1 G_{01} + X_2 G_{02})\,\mathbf{g}_{\rm psr} , \tag{3.23}$$

where $\mathbf{g}_{\rm psr}$ is the Galactic acceleration at the location of the pulsar system. In Eq. (3.22) v_T denotes the velocity of the pulsar system transverse to the line of sight, and d the distance between the solar system and the pulsar system. The effect of varying aberration reads

$$\frac{d\varepsilon_A}{dt} = -\frac{P_p}{P_b}\frac{1}{\sin i(1-e^2)^{1/2}}\frac{d}{dt}\left(\frac{\sin\eta}{\sin\lambda}\right) . \tag{3.24}$$

To make explicit Eqs. (3.19)–(3.21), we therefore need to know the values of the changes of the inclination, and of the polar angles of the spin of the pulsar, predicted by a generic theory of gravity. Both effects arise from coupling between the orbital and spin degrees of freedom, and they are therefore contained in the spin-orbit interaction Lagrangian (3.5c). The effects of spin-orbit coupling on secular evolution of the orbit have been worked out in general relativity in [56] and [38]. To generalize them to the present case it is sufficient to replace everywhere the combination $(\sigma_A)^{\rm GR}$ of Eq. (3.7) by the more general one, σ_A of Eq. (3.6b). Hence, we conclude that the orbit will rigidly precess in space with average vectorial velocity

$$\langle\mathbf{\Omega}^{\rm orbit}\rangle = \langle\mathbf{\Omega}_{\rm O}^{\rm orbit}\rangle + \langle\mathbf{\Omega}_{\rm SO}^{\rm orbit}\rangle , \tag{3.25}$$

where $\langle\mathbf{\Omega}_{\rm O}^{\rm orbit}\rangle = kn\mathbf{k}$ is the effect of the orbital Lagrangian (3.1), and where the effect of the spin-orbit interaction reads

$$\langle\mathbf{\Omega}_{\rm SO}^{\rm orbit}\rangle = \sum_{A=1}^{2}\langle\mathbf{\Omega}_A^{\rm orbit}\rangle , \tag{3.26a}$$

$$\langle\mathbf{\Omega}_A^{\rm orbit}\rangle = \frac{\sigma_A S_A}{a_R^3(1-e^2)^{3/2}}\,[\mathbf{s}_A - 3(\mathbf{k}\cdot\mathbf{s}_A)\mathbf{k}] . \tag{3.26b}$$

In these equations k is the orbital precession parameter, Eq. (3.10), $\mathbf{k} \equiv \mathbf{L}/|\mathbf{L}|$ is the direction of the orbital angular momentum [introduced in Eq. (2.13) as the third vector of the orbital triad], S_A is the magnitude of the spin of body A, and $\mathbf{s}_A \equiv \mathbf{S}_A/S_A$ the direction of its spin axis. These equations imply that the orbital inclination will undergo the secular variation

$$\frac{di}{dt} = \sum_{A=1}^{2}\frac{\sigma_A S_A}{a_R^3(1-e^2)^{3/2}}\,(\mathbf{s}_A\cdot\mathbf{i}) , \tag{3.27}$$

where $\mathbf{i} \equiv \mathbf{I} \equiv \mathbf{K}_0 \times \mathbf{k}/|\mathbf{K}_0 \times \mathbf{k}|$ is the direction of the ascending node, introduced in Eq. (2.13a). Note that the projection of the pulsar's spin on the nodal direction can

be expressed in terms of the polar angles λ and η as

$$\mathbf{s}_1\cdot\mathbf{i} = \mathbf{s}_1\cdot\mathbf{I} = \sin\lambda\,\cos\eta\ , \tag{3.28}$$

while the similar quantity for the contribution of the spin of the companion introduces new angles that had not yet entered our discussion, as well as the (unknown) magnitude of the spin of the companion. Fortunately, in the case of PSR 1913+16, and plausibly in many other cases, one can argue indirectly that the contribution of the spin of the companion S_2 is much smaller than that of S_1, because of the expected slowing down of a normal (nonrecycled) pulsar (see the discussion following Eq. (5.27) of Ref. [38], as further confirmed by the discussion between Eqs. (4.4)–(4.11) of Ref. [29]).

The final task that we need to address concerns the time evolution of the spin polar angles λ and η, which enter the timing parameters $\dot{x}^{\rm obs}$ and $\dot{e}^{\rm obs}$ indirectly through Eq. (3.24), and the pulse-structure parameters (2.26) directly. In other words, we wish now to discuss the effect of spin-orbit coupling on secular evolution of the pulsar spin. This evolution was derived within general relativity soon after the discovery of PSR 1913+16 [35, 56, 58–60]. To generalize these results to our generic theoretical framework, it is sufficient to remark that the spin-orbit Lagrangian (3.5c) couples the spin degrees of freedom to the orbital ones in the same linear way,

$$L'_{\rm SO} = -\sum_A \mathbf{\Omega}_A^{\rm spin}\cdot\mathbf{S}_A\ , \tag{3.29}$$

as is familiar for the interaction of a magnetic dipole with an external magnetic field. By a general mechanical argument [61], the derivative of $L'_{\rm SO}$ with respect to a vectorial rotation acting only on the rotational degrees of freedom of body A yields the mechanical torque acting on A:

$$\mathbf{K}_A = \partial L'_{\rm SO}/\partial\boldsymbol{\phi}_A = +\mathbf{\Omega}_A^{\rm spin}\times\mathbf{S}_A\ . \tag{3.30}$$

Hence the evolution of the spin of body A is given by

$$\frac{d\mathbf{S}_A}{dt} = \mathbf{\Omega}_A^{\rm spin}\times\mathbf{S}_A\ , \tag{3.31}$$

where

$$\mathbf{\Omega}_A^{\rm spin} = \frac{\sigma_A\mathbf{L}}{R^3}\ , \tag{3.32a}$$

$$\langle\mathbf{\Omega}_A^{\rm spin}\rangle = \frac{\sigma_A\mathbf{L}}{a_R^3(1-e^2)^{3/2}}\ , \tag{3.32b}$$

the latter equation giving the time average of the former one. From this Lagrangian derivation it is clear *a priori* that the total angular momentum $(\mathbf{L}+\Sigma\mathbf{S}_A)$ of the system will be conserved. (Indeed, the non-time-averaged precession of $\mathbf{L}$ is $d\mathbf{L}/dt = \Sigma\,\sigma_A\,\mathbf{S}_A\times\mathbf{L}/R^3$, see Ref. [38]). Working out the meaning of Eq. (3.31) in terms of the polar angles λ and η of $\mathbf{S}_1$ leads to

$$\frac{d\lambda}{dt} = -\,\Omega_1^{\rm spin}\sin i\,\cos\eta\ , \tag{3.33a}$$

$$\frac{d\eta}{dt} = +\,\Omega_1^{\rm spin}(\sin i\cot\lambda\,\sin\eta+\cos i)\ , \tag{3.33b}$$

with

$$\Omega_1^{\rm spin} = \frac{\sigma_1\mu(\mathcal{G}M)^{1/2}}{a_R^{5/2}(1-e^2)} = \frac{\mu}{M}\,\frac{c^2\sigma_1}{\mathcal{G}}\,\frac{\beta_O^2}{1-e^2}\,n\ . \tag{3.34}$$

Of particular interest is the time evolution of the combination $\sin\eta/\sin\lambda$ appearing in the aberration effect (3.24). It is given by

$$\frac{d}{dt}\left(\frac{\sin\eta}{\sin\lambda}\right) = \frac{\Omega_1^{\rm spin}}{\sin^2\lambda}(\,\sin i\,\cos\lambda\,\sin 2\eta + \cos i\,\sin\lambda\,\cos\eta)\ . \tag{3.35}$$

We find it useful to remember that in general relativity the ratio of $\Omega_1^{\rm spin}$ to the periastron precession $\dot{\omega} = kn$ is 7/24 ($\simeq 0.29$) in the equal-mass case. Note also that an aligned rotator with $\mathbf{s}_1 = +\mathbf{k}$ corresponds to $\lambda = i$ and $\eta = -\pi/2$, for which values the right-hand sides of Eqs. (3.33) and (3.35) vanish. Furthermore, if we denote by δ $(0\le\delta<\pi)$ the "misalignment," i.e., the angle between $\mathbf{s}_1$ and $\mathbf{k}$ $(\mathbf{k}\cdot\mathbf{s}_1 = \cos\delta)$, and by $\phi_{\rm SO}$ the longitude of $\mathbf{s}_1$ during its precession motion around $\mathbf{k}$ (counted in the sense of motion from the meridian defined by $-\mathbf{J}$), we have

$$\cos\lambda = \cos\delta\cos i - \sin\delta\sin i\cos\phi_{\rm SO}\ , \tag{3.36a}$$

$$\cos\eta = \sin\delta\sin\phi_{\rm SO}/\sin\lambda\ , \tag{3.36b}$$

in which δ is fixed in time while $\phi_{\rm SO} = +\Omega_1^{\rm spin}t + {\rm const.}$ Although the direction of $\mathbf{s}_1$ can be equivalently described by $(\delta,\phi_{\rm SO})$ instead of (λ,η), we shall use the latter pair of angles because they are more directly related to measurable quantities.

In addition to providing expressions for the values of $\dot{e}^{\rm obs}$ and $\dot{x}^{\rm obs}$, the results (3.33) allow one to derive explicit equations for the secular-drift pulse parameters $\dot{\lambda}$, $\dot{\kappa}$, $\dot{\sigma}$, $\dot{\kappa}'$, $\dot{\sigma}'$, and $\dot{\psi}_0$ in the set (2.26). When computing these it is useful to keep track of their order of magnitude in terms of two basic small parameters: the ratio $v^{\rm orbital}/c$, which can be approximated by β_O, Eq. (3.8b), and a corresponding ratio for the equatorial spin velocity of the pulsar, say $\beta_S = cS/Gm^2$ [38]. Then we have

$$\dot{\omega}/n \sim \Omega^{\rm spin}/n \sim \beta_O^2\ , \tag{3.37a}$$

$$\Omega_{\rm SO}^{\rm orbit}/n \sim \beta_O^3\beta_S\ , \tag{3.37b}$$

$$(d\varepsilon_A/dt)/n \sim \beta_O^5\beta_S^{-1}\ , \tag{3.37c}$$

$$[\Omega^{\rm GW}/n]^{\rm GR} \sim \beta_O^5\ . \tag{3.37d}$$

For the pulsars PSR 1913+16 and PSR 1534+12 one has roughly $\beta_O\sim\beta_S\sim 2\times10^{-3}$, which shows that the indirect spin-orbit contributions to $\dot{x}^{\rm obs}$ and $\dot{e}^{\rm obs}$ should be appreciably greater than the gravitational-wave damping contributions.

C. Post-Keplerian parameters and tests of relativistic gravity

To simplify the following discussion we shall assume that, beyond the Keplerian parameters, one has already

extracted from some pulsar data both the secular periastron advance parameter, $\dot{\omega} \equiv kn$, and the time dilation parameter, $\gamma \equiv e\delta/n$. From Eqs. (3.8)–(3.11) it is clear that, in each theory of gravity, these two measurements will constrain the two unknown masses to lie at the intersection of two curves in the m_1, m_2 plane. The shape and position of the curves will depend on the strong-field effects contained in $\mathcal{G} \equiv G_{12}$, $\varepsilon \equiv \varepsilon_{12}$, and ξ defined by Eq. (3.6a), as well as on the parameter η^* measuring the sensitivity of the local value of the (test-particle) gravitational coupling constant to some external gravitational potential. Although, in general, we need to measure at least three PK parameters to have a sharp test of gravity theories, the measurement of even two of them, e.g., $\dot{\omega}$ and γ, can still provide interesting limits on how far a theory can deviate from the correct theory through the simple requirement that the corresponding two curves in the mass plane must intersect. We shall see below that this requirement provides nontrivial limits on the free parameters of a rather general class of tensor-biscalar theories. Assuming henceforth that the intersection requirement is satisfied, we can now discuss what the measurement of any further PK parameters, beyond $\dot{\omega}$ and γ, can teach us about gravity.

1. *Orbital period derivative, $\dot{P}_b$*

Equations (3.10)–(3.17) help to clarify what was emphasized in the Introduction: that combining a measurement of $\dot{P}_b$ (which in a clean binary system is predominantly determined by gravitational-wave damping) with measurements of $\dot{\omega}$ and γ gives access to a mixed test wherein both radiative and quasistatic strong-field effects play important roles. As recently shown by Damour and Esposito-Farèse [32], this mixing of effects allows theories that differ significantly from general relativity to pass the test just as satisfactorily as relativity itself. Moreover, Eqs. (3.19), (3.22) and the recent work of Damour and Taylor [29] show that the $\dot{D}$ contribution to $\dot{P}_b$ can ultimately limit the precision of the tests of relativistic gravity deducible from $\dot{P}_b$ (or, alternatively, the precision with which one can phenomenologically constrain the time variation of Newton's gravitational constant G [62]). In particular, the relatively poor accuracy with which one knows the basic Galactic quantities v_0 and R_0 (with $g_{\rm solar} = v_0^2/R_0$) will within a few years dominate the overall uncertainty in interpreting $\dot{P}_b$ for PSR 1913+16, at a level of about 0.2% of the total observed effect.

Fortunately, the Galactic source of uncertainty is considerably reduced for relatively nearby binary pulsars such as PSR 1855+09 and PSR 1534+12. Here we assume that $G^{-1}(X_1 G_{01} + X_2 G_{02}) \simeq 1$ in Eq. (3.23), so that for $d \ll R_0$ one gets mainly the differential Galactic acceleration $\mathbf{g}_{\rm psr} - \mathbf{g}_{\rm solar} \propto d$, see Eq. (2.8) of Ref. [29]. On the other hand, one must still worry about subtracting the transverse-velocity effect v_T^2/cd, which might then become the major source of uncertainty. These issues call attention to the desirability of planning observations of nearby pulsars so as to facilitate direct measurement of both the proper motion ($\mu = v_T/d$) and the annual parallax ($\pi = 1/d$), either from timing data or by other means.

2. *Shapiro delay parameters, r and s*

Equations (3.14) and (3.15) show that measurements of r and s can provide two clean tests of the strong-field effects entering the pure orbital, $O(v^2/c^2)$-accurate Lagrangian, Eq. (3.1).

3. *Orbital shape correction, δ_θ*

Equations (3.13) and (3.18) show that measurement of δ_θ provides a test of gravity only if we know, from some other evidence, the direction $\mathbf{s}_1$ of the spin axis of the pulsar. Such evidence is already available for PSR 1913+16: studies of secular evolution of its pulse structure [63, 64] indicate that $\mathbf{s}_1$ is probably aligned with $\mathbf{k}$ to within a few degrees, so that $\lambda \simeq i$ and $\eta \simeq -\pi/2$. Alternatively, a measurement of δ_θ can provide a handle on the direction in space of $\mathbf{s}_1$, which can be of interest for the spin-orbit tests discussed below.

4. *Derivative of orbital eccentricity, $\dot{e}$*

From Eqs. (3.21) and (3.24), and assuming for simplicity that the gravitational-wave contribution to $\dot{e}$ can be neglected, we see that a measurement of $\dot{e}$ can provide a significant test of the precession of $\mathbf{s}_1$ due to spin-orbit interaction.

5. *Derivative of projected semimajor axis, $\dot{x}$*

From Eqs. (3.20), (3.24), and (3.27), and assuming also for simplicity Eqs. (3.37), we see that a measurement of $\dot{x}$ is a test of the combined influence of spin-orbit coupling on the spin, Eqs. (3.24) and (3.35), as well as on the orbit, Eq. (3.27) [38].

6. *Pulse-structure parameters*

Among the pulse-structure parameters, those most likely to be measurable are α, $\lambda \equiv \pi - \zeta$, and ψ_0. Here we assume the favorable circumstances in which polarization and pulse-shape information are available over a wide range of pulsar phase; otherwise it may be possible to measure only the angular distance between the magnetic axis and the line of sight, i.e., the "impact parameter" $\zeta - \alpha$ [52, 65]. Knowledge of λ is very useful, because $|\lambda - i|$ provides a lower limit for the angle between $\mathbf{s}_1$ and $\mathbf{k}$ and therefore a lower limit on the amplitude of spin-orbit precession in the system. (Recall, however, that i is generally known only modulo the ambiguity $i \to \pi - i$.) More information is needed to determine η, the other polar angle of $\mathbf{s}_1$. As indicated by Eq. (2.23), even the precise removal of Faraday rotation from the observed central polarization angle ψ_0 is not sufficient, because of the added contribution of the unknown longitude of the ascending node Ω (which does not otherwise enter the

relations between PK parameters, although it does play an important role in some relativistic orbital properties of binary pulsar systems in presence of a violation of the strong equivalence principle [39]). This dependence illustrates the importance of trying to extract more parameters from pulse-structure observations.

As first pointed out by Smarr and Blandford [49], the parameters κ and σ of Eqs. (2.27), which enter the aberration-induced periodic shift of ζ,

$$\delta_A\zeta = \beta_1[-\kappa S(u) + \sigma C(u)] , \tag{3.38}$$

give access in a single orbit to the angle η [modulo the ambiguity indicated following Eqs. (2.28)]. Moreover, as we pointed out in Sec. II B above, polarization measurements can, in principle, determine the parameters κ' and σ' entering the aberration-induced shift of ψ_0, Eqs. (2.24) and (2.28). These parameters would give access to both λ and η (modulo some discrete ambiguities), and repeated observations of pulse structure over many years could in principle give access to the secular drifts $\dot{\lambda}$, $\dot{\psi}_0$, $\dot{\kappa}$, $\dot{\sigma}$, $\dot{\kappa}'$, and $\dot{\sigma}'$. Such redundant measurements would provide (at least within the assumptions of the rotating pole model) several tests of the relativistic precession of a spinning neutron star in an arbitrary theory of gravity [Eqs. (3.33)], thereby complementing and going beyond weak-field tests of gravitomagnetic effects.

Note that even if aberration effects are too small to give access to κ and σ (or κ' and σ') and their drifts, the combined measurements of λ, ψ_0, $\dot{\lambda}$ and $\dot{\psi}_0$, if complemented by an accurate removal of Faraday rotation, could yield (modulo some sign ambiguities) values for η and $\Omega_1^{\rm spin}$, and thereby a test of relativistic gravity. Indeed, as seen from Eqs. (3.37) above and Eq. (5.11b) of Ref. [38], the $d\Omega/dt$ contribution to $\dot{\psi}_0$ is negligible compared to the $d\eta/dt$ one. Therefore we would know at once λ, $\dot{\lambda}$, and $d\eta/dt$, and we could use Eqs. (3.33) to determine both η and $\Omega_1^{\rm spin}$ (modulo some discrete ambiguities). More precisely, let us consider as an example the case where the misalignment angle δ is small but nonzero. Since $(-\sin\eta) = \cos(\eta + \pi/2) = 1 + O(\delta^2)$, we can consistently approximate $\sin\eta$ by (-1) on the right-hand side of Eq. (3.33b), providing the value of $\Omega_1^{\rm spin}$ in terms of $d\eta/dt$, λ, and i. Equation (3.33a) can then be used to determine η. This example (which is probably relevant to many real cases) shows that monitoring the secular evolution of ψ_0 is physically important because it can lead, in contrast with the measurement of $\dot{\lambda}$, to a direct measurement of $\Omega_1^{\rm spin}$, and therefore to a test of relativistic gravity.

IV. MEASURABILITY OF POST-KEPLERIAN PARAMETERS

A. General concept of measurability

Before exhibiting specific examples of how well (or how poorly) some parameters can be measured starting from pulsar data, let us briefly discuss our general approach to the issue of measurability of fitted parameters. The two basic elements of the problem under discussion are (1) a finite sequence of observed arrival times on Earth, $t_i^{\rm obs}$, $i = 1, \ldots, N$, each endowed with a one-σ observational "error bar" $\sigma^{\rm obs}$, and (2) a theoretical model, i.e. an explicit mathematical function, say F, of one integer n and a set of parameters $\{p_\alpha\}$ which predicts that, in absence of noise, and for the actual values of the parameters, $p_\alpha^{\rm act}$, the nth pulse should arrive on Earth at time $t^{\rm theor}(n) = F(n; p_\alpha^{\rm act})$. As a particular example we note that the actual data set for PSR 1913+16 has $N = 4926$ measured pulse arrival times as of December 1990, and that most of the 3713 recorded since 1981 have $\sigma_i^{\rm obs} \approx 15\,\mu$s. Approximately 20 parameters p_α are required in fitting these observations to the theoretical model [22].

Because of noise in the observations, there would not be perfect agreement between observed and theoretical arrival times even if we knew in advance the actual values of the p_α's. Moreover, we do not know the actual values of the p_α's; the best we can do is to choose a definite algorithm allowing us to compute from the set of noisy data $\{t_i^{\rm obs}, \sigma_i^{\rm obs}\}$ a set of estimated parameters $\{p_\alpha\}$, say

$$p_\alpha^{\rm est} = E_\alpha(t_i^{\rm obs}, \sigma_i^{\rm obs}) . \tag{4.1}$$

Note that the choice of pointwise estimators E_α is partly arbitrary, though restricted by the basic consistency requirement that $p_\alpha^{\rm est}$ should converge, in probability, to $p_\alpha^{\rm act}$ when the number of observations tends to infinity or the variances to zero. (See, e.g., Levine [66] for a thorough discussion of the various other requirements that one may wish to impose on statistical estimates.) Having chosen the estimators E_α, it is important to keep in mind that the parameter values $p_\alpha^{\rm est}$, defined by Eq. (4.1) are random variables that inherit their probabilistic characteristics (distribution function in the space of the p_α's) from the ones of the noisy data $t_i^{\rm obs}$, supposed to be an arbitrary sample selected from a random process with known statistical characteristics. In the following we shall assume that the noise in $t_i^{\rm obs}$ is uncorrelated (for different values of i) Gaussian noise, with standard deviations $\sigma_i^{\rm obs}$.

Given the observations, their noise characteristics, and some estimators E_α, we can describe quantitatively the measurability of each parameter p_α by the size of suitable confidence intervals of its corresponding random variable $p_\alpha^{\rm est}$, defined by Eq. (4.1). We then state that p_α is "measurable" from the data $\{t_i^{\rm obs}, \sigma_i^{\rm obs}\}$ if, say, a 90% confidence interval of $p_\alpha^{\rm est}$ is contained within some physically interesting target interval. The absolute and/or fractional size of the interval will depend not only on the considered parameter, but also on the theoretical framework within which one chooses to interpret it. Usually, the target interval for a nonzero parameter could be something like $[\frac{1}{2}p_\alpha^{\rm pred}, 2p_\alpha^{\rm pred}]$, or sometimes $[-2p_\alpha^{\rm pred}, +2p_\alpha^{\rm pred}]$, where $p_\alpha^{\rm pred}$ is a "predicted" value for p_α, given previous measurements of other, more easily measurable, parameters in the set $\{p_\alpha\}$ and some standard physical theory linking the p_α's among themselves. (This would, for example, be the case for the parameter r, given previous measurements of $\dot{\omega}$ and γ and working within the standard general relativistic framework.) However, if the

standard theory predicts a zero or unobservably small value for some parameter p_α, but a nonstandard theory predicts a relatively large value, the choice of a correspondingly large target interval will still entitle us to make a significant measurement of this parameter, leading to a solid test of the nonstandard theory.

In the following discussion we shall use least-squares estimators, defined by taking for $p_\alpha^{\rm est}$ the (generally unique) values of parameters that, for given data $\{t_i^{\rm obs},\ \sigma_i^{\rm obs}\}$, minimize the quantity

$$\chi^2(t_i^{\rm obs},\ \sigma_i^{\rm obs};p_\alpha)\ =\ \sum_{i=1}^{N}\left(\frac{t_i^{\rm obs}-F(n_i;p_\alpha)}{\sigma_i^{\rm obs}}\right)^2 . \quad (4.2)$$

In this expression n_i denotes the number of the pulse observed at time $t_i^{\rm obs}$, defined as the integer which minimizes the difference $|t_i^{\rm obs}-F(n_i;p_\alpha)|$. (In the actual implementation of the least-squares algorithm, it is convenient to approximate the differences $t_i^{\rm obs}-F(n_i;p_\alpha)$ by $P_p[G(t_i^{\rm obs};p_\alpha)-n_i]$, where G is the inverse of function F, i.e., $F[G(t,p_\alpha);p_\alpha]\equiv t$; see Ref. [22].) In addition to its consistency and other good statistical properties, the least-squares procedure has the advantage of leading, at least in favorable cases, to a simple description for the statistical properties of the estimated parameters. Indeed, when the noise in $t_i^{\rm obs}$ is Gaussian with standard deviation $\sigma_i^{\rm obs}$, and when N is sufficiently large, the level contours in the space of fitted parameters of the function

$$\Delta\chi^2(p_\alpha)\equiv\chi^2(p_\alpha)-\inf_{p_\alpha}\chi^2(p_\alpha)\equiv\chi^2(p_\alpha)-\chi^2(p_\alpha^{\rm est}) \quad (4.3)$$

correspond to known confidence levels which depend only on the number of fitted parameters one is concentrating upon. For example, if one is interested in the separate measurability of one particular parameter, say p_1, the condition $\Delta\chi^2<1$ defines a 68% confidence interval containing $p_1^{\rm est}$, while $\Delta\chi^2<4$ defines a 95% confidence interval. For the joint measurability of two parameters, p_1 and p_2, 68% and 95% confidence regions are enclosed by the level contours $\Delta\chi^2=2.3$ and $\Delta\chi^2=6.2$, respectively. This simple description is valid when N is large enough, or the σ_i's small enough, that the shape of the $\Delta\chi^2(p_\alpha)$ function around its minimum is parabolic in all relevant directions of parameter space. When this is not the case for some directions, which means that some parameters are not well measurable, it is still convenient to use the successive $\Delta\chi^2$ contours to define confidence regions and to quote the corresponding standard probabilities as nominal confidence levels.

B. Preliminary analysis

As a first way of gauging the measurability of some parameters, it is convenient to use simple approaches before studying the full variation in parameter space of the $\chi^2(p_\alpha)$ function (4.2). One simple approach consists of fitting the data $\{t_i^{\rm obs},\sigma_i^{\rm obs}\}$ to models differing in the presence of parameters known to correspond to small effects, and therefore expected to be measurable only with difficulty. For example, we know *a priori* that the BT model was conceived so as to contain, beyond the basic Keplerian orbit, only the largest post-Keplerian effects present in timing data, namely those associated with a secular advance of the periastron $\dot\omega$ and time dilation γ, in addition to various other possible secular drifts of Keplerian parameters ($\dot P_b$, $\dot e$, $\dot x$). By contrast, the DD model was designed to complete the BT model by including all conceivable (within a large class of theories) secular and periodic relativistic timing effects at the fractional level $(v^{\rm orbit}/c)^2$ beyond the Keplerian ones, neglecting only $(v^{\rm orbit}/c)^3$ effects (expected to contribute only at the negligible 30 ns level for $v^{\rm orbit}/c<3\times10^{-3}$). A simple way of estimating in advance whether or not the new (separately measurable) parameters appearing in the DD model (namely r, s, δ_θ) will be measurable, is to compare the quality of the fit of some given data to the BT and DD models. A first, global, measure of the goodness of fit is simply the minimum value of χ^2, say $\chi^2_{\rm min}$, after all fitted parameters have been optimized. We know that when the number of measurements N is sufficiently large, $\chi^2_{\rm min}$ can be approximated by a Gaussian random variable of mean value $N-\nu$ and variance $2(N-\nu)$, where ν denotes the total number of fitted parameters and $N-\nu$ the number of degrees of freedom. Table I exhibits the values of $N-\nu$ and $\chi^2_{\rm min}$ for fits of actual timing data to the BT and DD models [22, 23, 42]. The numbers show that the DD model is a significantly better fit to the data than the BT one, which would seem to imply that some of the new parameters appearing in DD must be readily measurable. [Note that it is mostly the difference $\chi^2_{\rm min}({\rm BT})-\chi^2_{\rm min}({\rm DD})$ that is significant; the fact that $\chi^2_{\rm min}({\rm DD})$ exceeds $N-\nu$ by about twice $\sqrt{2(N-\nu)}$ is a consequence of imprecise estimates of the experimental uncertainties in the data.]

However, this conclusion regarding measurability is not quite correct for the following reason. The DD model differs from the BT one in two ways: it introduces new parameters corresponding to effects not included in BT, but it also associates more effects with "old" parameters than BT does. Such is notably the case for the parameter associated with the periastron advance, denoted $\dot\omega$ in BT and k in DD (with $\dot\omega=nk=2\pi k/P_b$). In the BT model, $\dot\omega$ takes into account only the secular drift of the longitude of periastron, $\omega_{\rm BT}=\omega_0+\dot\omega(t-t_0)$, whereas in the DD model k describes both the secular drift and the quasiperiodic motion according to $\omega_{\rm DD}=\omega_0+kA_e(u)$. (See Secs. 3.6 and 3.9 of [36] for a full discussion of this issue.) This situation suggests defining an improved version of the BT model, say BT+, which does not con-

TABLE I. Values $N-\nu$ and $\chi^2_{\rm min}$ for observations of PSR 1913+16 fitted to three different timing models.

Model	Degrees of freedom $(N-\nu)$	$\chi^2_{\rm min}$
BT	3697	3969.5
BT+	3697	3890.2
DD	3697	3878.9

tain more parameters than BT, but which associates with $\dot{\omega}$ the full secular-plus-periodic effects of periastron advance by using everywhere $\omega_{\rm DD}$ instead of $\omega_{\rm BT}$. One sees in Table I that the BT+ model fits the PSR 1913+16 data nearly as well as does the DD model. This result shows that previous reports ([21], and especially Fig. 6 of [22]) of a significant measurement of a "post-BT" parameter (respectively $(\sin i)_{\rm EH}$ and $(\sin i)_{\rm H88}$ in Refs. [21, 22]) were mainly consistency checks that the periastron advance contains, as predicted by all relativistic theories of gravity, both secular and quasiperiodic effects as described by Eqs. (2.3).

Beyond realizing from comparison of the values of $\chi^2_{\rm min}$ in the BT+ and DD models that the global measurability of the new post-Keplerian parameters contained in DD is much smaller than one might think, one can try to exhibit more explicitly the actual magnitude of the timing effects contained in DD but not in BT+. This can be done by numerical simulation in the following way. One first generates mock timing observations by adding (pseudo-)random Gaussian noise to a sequence of theoretical arrival times computed within the DD model, using general relativistic predictions for the unmeasured PK parameters. Then one fits the fake data to the BT+ model and plots the residuals as functions of the orbital phase.

For illustrative purposes, we plot such residual difference curves in Fig. 2(a) for both "DD–BT" and "DD–BT+", using the current orbital parameters of the PSR 1913+16 system. Although the DD–BT curve [dashed line in Fig. 2(a)] has a maximum amplitude $> 5\,\mu$s, most of it arises from the nutation in the periastron advance. After this effect is accounted for, the DD–BT+ curve (solid line) shows that in general relativity the post-BT+ parameters produce a "useful signal" currently amounting to only 0.4 μs. The useful signal strength turns out to vary with the mean value of ω_0 in the data set. For PSR 1913+16 it was much larger some years ago, approximately $2\,\mu$s in 1975, when $\omega_0 = 180°$; it will reach a minimum of less than $0.1\,\mu$s in 1996, when $\omega_0 = 270°$, before increasing again. Since the current observational precision for PSR 1913+16 is about $15\,\mu$s, the prospects for measuring new PK parameters from its timing data are not very good, at least on a short time scale. (Nevertheless, we shall see in Sec. V that PSR 1913+16 can still provide significant new constraints on specific classes of alternative relativistic gravity theories.)

For comparison, Fig. 2(b) exhibits the residual differences DD–BT and DD–BT+ for data simulating the recently discovered binary pulsar PSR 1534+12. In this case the two residual difference curves are nearly identical, which implies that for this set of orbital parameters the new effects contained in the DD model produce an observable signal associated mainly with the extra parameters r, s, and δ_θ rather than with the "nutation" $\omega_{\rm DD} - \omega_{\rm BT}$ in the periastron advance. (The main physical difference between the parameters of PSR 1534+12 and those of PSR 1913+16 responsible for this improvement is a much greater inclination of the orbital plane, $\sin i \approx 0.96$ as opposed to 0.73, which amplifies and renders more recognizable the Shapiro time delay.) Most

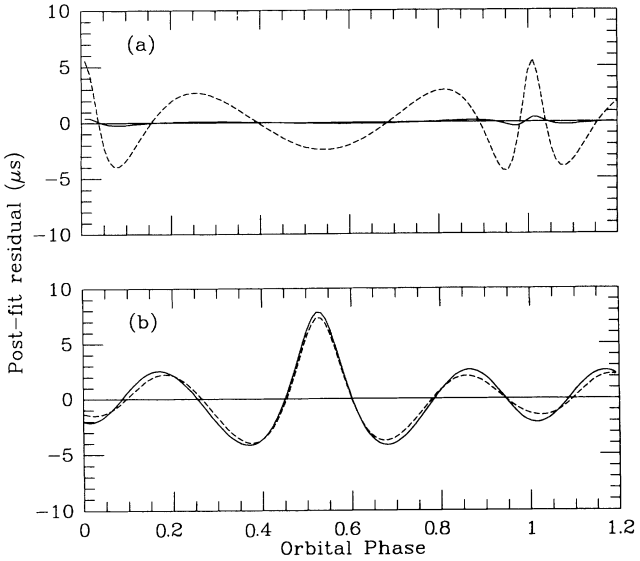

FIG. 2. Post-fit residual differences between the DD and BT models (dashed lines), and the DD and BT+ models (solid lines), obtained by using the orbital parameters of (a) PSR 1913+16 and (b) PSR 1534+12. Mock data were generated using equations of the DD model and the currently observed parameters of each pulsar; the data were then fitted to the BT and BT+ models by adjusting the Keplerian orbital parameters, and the residuals were connected with straight line segments.

importantly, Fig. 2(b) shows that for PSR 1534+12 the useful signal associated with the new set of PK parameters $\{r, s, \delta_\theta\}$ is about $8\,\mu$s in general relativity, appreciably greater than the precision of the timing observations (currently around $3\,\mu$s for 5-min observations, with good prospects for further improvement). From this simple preliminary analysis we conclude that it should already be possible to extract some yet unmeasured post-Keplerian parameters among the set $\{r, s, \delta_\theta\}$, using existing timing data for PSR 1534+12. These parameters will immediately provide qualitatively new tests of relativistic gravity: in particular, tests specifically of the gravitational interaction in the quasistationary strong-field regime.

C. Measurability of timing parameters

As a consequence of the general approach outlined in Sec. IV A, the question of measurability of the PK parameters from timing data boils down to mapping out the shape of the $\chi^2(p^{\rm PK})$ surface around its global minimum, $\chi^2_{\rm min}$. Such a mapping was carried out for the two PK parameters r and s, for PSR 1913+16, by Taylor and Weisberg (see Fig. 7 of [22]). Their analysis confirms the intuitive conclusion reached by studying the residual difference DD–BT+, namely, that the useful signal associated with r and s is so small as to render these parameters not separately measurable for this pulsar at present. In order to explore this issue further, and to extend our understanding of parameter measurability to other binary

pulsars, including ones yet to be discovered, we carried out a series of numerical simulations with mock pulsar data. The simulations include cases specifically designed to show what might be learned from improved and extended observations of PSR's 1913+16 and 1534+12, as well as results for "generic" binary pulsars with a wide range of orbital parameters.

The simulations for PSR 1913+16 were carried out by generating fake data using the DD timing model and the measured parameters of this pulsar, plus general-relativistic predictions for the unmeasured PK parameters. The basic data set extended over 10 years, with one 2-h "observing session" per month; each session provided 24 values of $t_i^{\rm obs}$, to which we added Gaussian noise with 1 μs root-mean-square amplitude. We carried out least-squares solutions in the same way as for real observations, and recorded the estimated fractional uncertainties of the PK parameters corresponding to the $\Delta\chi^2 < 1$ multiparameter confidence region. Figure 3 illustrates the results plotted as a function of ω_0, the assumed longitude of periastron near the midpoint of the 10-yr data span. In this simulation 20 parameters were estimated, and among the separately measurable PK parameters (2.1c) only $\dot{x}$ was fixed (to zero) after previous simulations had shown the difficulty of measuring it with interesting accuracy. Note that all parameter uncertainties scale linearly with the uncertainties in the data, and note also that the standard 1 μs noise for 5-min integrations used in the simulations is considerably smaller than the experimental accuracies currently being achieved for PSR 1913+16. (However, the planned upgrading of the Arecibo telescope might make such accuracies achievable within a few years.)

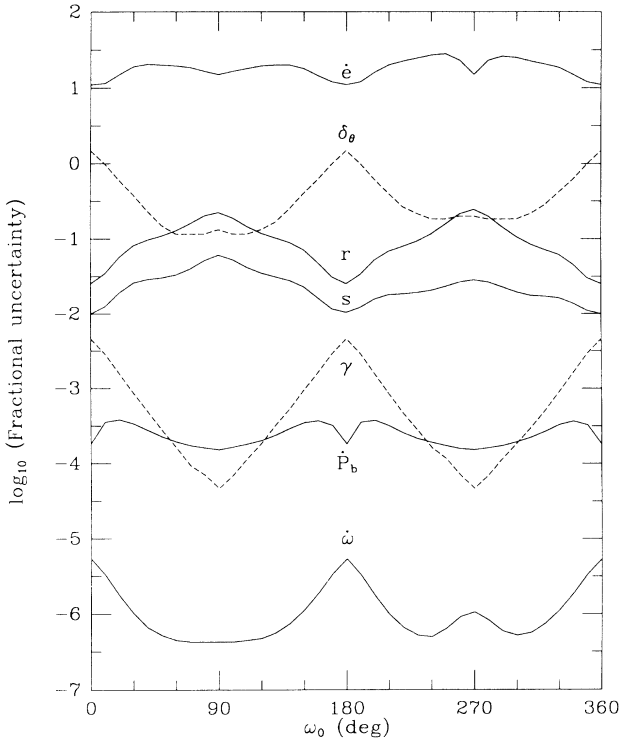

FIG. 3. Fractional uncertainties of seven post-Keplerian parameters, estimated from simulated observations of PSR 1913+16 in which 20 parameters were fitted. The generated data contained 1 μs of random noise, and included 24 consecutive five-minute "observations" taken once per month for 10 yr, for a total of 2880 pulse arrival times. The target value of each parameter was taken to be its computed (or plausible) value in general relativity, based on the measurements of [22, 23]. In particular, we used $(\delta_\theta)^{\rm target} = 6 \times 10^{-6}$ and $(\dot{e})^{\rm target} = 2 \times 10^{-17}$ s^{-1}.

Since the PSR 1913+16 system had $\omega_0 \approx 226°$ in 1986, Fig. 3 "predicts" that the available real observations, which include 10 years of measurements starting in 1981 with $\sigma_i^{\rm obs} \approx 15\,\mu$s, should yield very good measurements of $\dot{\omega}$, γ, and $\dot{P}_b$ in addition to fractional uncertainties around 1.0 and 0.3 for r and s, respectively. These predictions are borne out by the experimental results of Taylor and Weisberg [22]. One may also infer from Fig. 3 that r and s could become separately measurable, in the future, if improved techniques reduce the observational uncertainties by an appreciable factor. With higher precision and longer data spans, even the parameter δ_θ might become measurable. Because pulse-structure observations indicate that the spin axis of PSR 1913+16 is nearly aligned with the orbital angular momentum [63, 64], one already knows reasonably well the angles entering the unmeasurable aberration parameters A and B [Eqs. (3.16) and (3.17)], namely $\lambda \simeq i$, $\eta \simeq -\pi/2$. Therefore even a coarse measurement of δ_θ would constitute a new strong-field test of relativistic gravity, complementing the two others potentially available through more precise measurements of r and s.

We explored the dependence of PK-parameter measurability on the total span T of the observations (when keeping fixed the data-acquisition rate). Three of the PK parameters measure signals whose amplitudes grow linearly ($\dot{\omega}$, $\dot{e}$) or quadratically ($\dot{P}_b$) with time, so one expects these parameters to become progressively easier to measure with larger T. Furthermore, γ and δ_θ become reasonably orthogonal to the rest of the model only on the time scale of orbital precession, $2\pi/\dot{\omega} \simeq 85$ yr for PSR 1913+16, so their measurability also improves rapidly with time. On the other hand r and s, like the Keplerian orbital parameters, are in principle measurable with data from a single orbit; for these parameters, additional observations are advantageous only insofar as they help to average down the noise. In general we find that for intervals T well below the orbital precession period, uncertainties in the PK parameters scale approximately as T^a, with the exponents a listed in columns 2 and 3 of Table II. These scaling rules can be used together with the results in Fig. 3 to estimate, for example, that 20 more years of 15-μs data for PSR 1913+16 (in addition to the 10 years already in hand) should provide a 22% measurement of δ_θ.

We now turn our attention to the newly discovered binary pulsar PSR 1534+12. The exploratory analysis of Sec. IV B clearly illustrated this object's potential for yielding good measurements of two new PK parameters, r and s. With our appetites whetted, we carried out a series of numerical simulations for this pulsar, obtaining the results summarized in Fig. 4. Again the simulations

TABLE II. Dependence of fractional parameter uncertainties on T^a and $(P_b)^b$, computed by numerical simulations and by analytical approximations.

Parameter	a		b	
	Numerical	Analytical	Numerical	Analytical
$\dot{\omega}$	−1.3	−3/2	1.1	1
γ	−1.5	−3/2	1.4	4/3
$\dot{P}_b$	−2.3	−5/2	3.0	3
r	−0.5	−1/2	0.0	0
s	−0.5	−1/2	0.0	0
δ_θ	−2.3	−5/2	3.2	10/3

assumed 10 years of once-per-month observations with timing accuracies of 1 μs in 5 min, and $\dot{x}$ was fixed to zero. Figure 4 and Table II show that at the present $\omega_0 \approx 264°$, simultaneous measurements of r and s, in addition to $\dot{\omega}$ and γ, should already be possible by using the available one year of 3–5 μs data [41,42]: we can predict fractional accuracies of order $\sigma_s/s \simeq 10^{-2}$, $\sigma_r/r \simeq 10^{-0.8}$. Thus, observations of PSR 1534+12 can already give access to two important tests of strong-field gravity.

Figure 4 and Table II also show that within a few years $\dot{P}_b$ will be measurable at the general relativistic target level, $\dot{P}_b^{\rm GR} \simeq -1.92 \times 10^{-13}$. As emphasized in Sec. III C above, a clear interpretation of the $\dot{P}_b$ measurement will also require reliable measurements of the proper motion μ and annual parallax π. Our simulations suggest that within several years μ could be determined to a few percent, and π to perhaps 20% accuracy. On the other hand, even after 10 years of 1-μs data, δ_θ will be measurable for PSR 1534+12 only to within a factor 3, probably too coarse to be of interest. Observations over 30 yr with 1-μs accuracy might permit δ_θ to be determined to 20%, and $\dot{e}$ to a level of 2×10^{-17} s^{-1}, the general-relativistic target level for reaching a timing-data measurement of $\cos\eta$ according to Eqs. (3.21), (3.24), and (3.35).

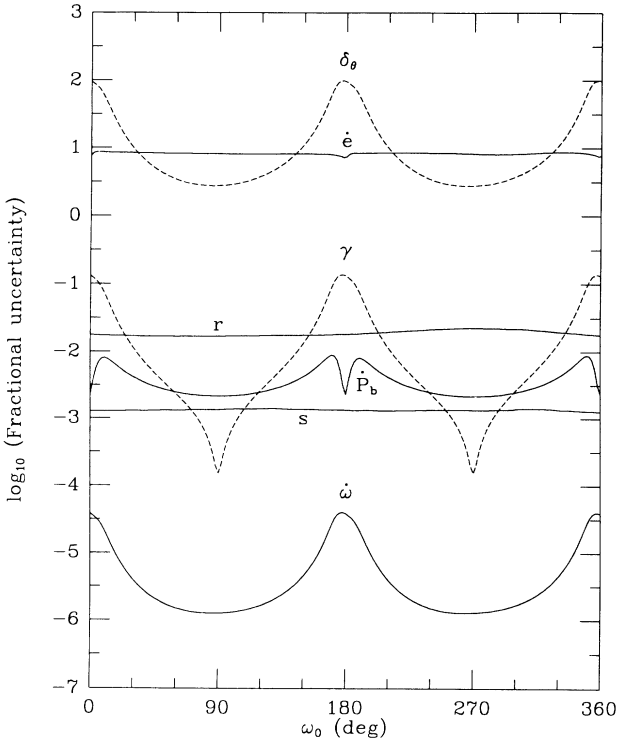

FIG. 4. Fractional uncertainties of seven post-Keplerian parameters, estimated from simulated observations of PSR 1534+12. The simulation procedure was similar to that used for PSR 1913+16 (see caption of Fig. 3), and the assumed orbital parameters were those given in Ref. [41]. We used general-relativistic target values $(\delta_\theta)^{\rm target} = 5 \times 10^{-6}$, $(\dot{e})^{\rm target} = 2 \times 10^{-17}$ s^{-1}.

In order to permit rapid evaluation of the relativistic implications of future binary pulsar discoveries, we also carried out simulations for a wide range of "generic" orbital parameters. To cut down on the number of simulations we assumed pulsar and companion star masses $m_1 = m_2 = 1.4\,M_\odot$, close to the values observed in the PSR 1913+16, 2127+11C, and 1534+12 systems, and a fixed data-acquisition rate with 2-h mock "observing sessions" carried out once per month. We determined that the dependence of parameter measurabilities on orbital period P_b can be approximately factored out as a power $(P_b)^b$, similarly to the scalings T^a discussed above. The scaling laws were established both analytically and by means of numerical tests using 10-yr data spans and orbital periods in octave steps from 2 to 256 h. The exponents a and b expressing the scalings of the fractional uncertainties in the parameters $\dot{\omega}$, γ, $\dot{P}_b$, r, s, and δ_θ when T and P_b change are displayed in Table II. (Note that the scaling laws may be inaccurate for short data spans if the orbital orientation is close to $\omega_0 = 0°$ or 180°.) Using a fixed orbital period of 10 h and a three-dimensional grid of other parameter values defined by

$$\omega_0 = 0, 15°, \ldots, 360°\,, \tag{4.4a}$$

$$e = 0.1, 0.2, \ldots, 0.9\,, \tag{4.4b}$$

$$c \equiv \sqrt{1 - s^2} = 0.05, 0.15, \ldots, 0.95\,, \tag{4.4c}$$

we then carried out 2250 simulated solutions and recorded the estimated uncertainties of the PK parameters for each one. [Note that our choice of a uniform sampling in the values of $c \equiv |\cos i|$ is motivated by the fact that the *a priori* probability of observing an inclination in the interval $(i, i + di)$ is $\frac{1}{2}\sin i\, di$.]

Results of the generic simulations are summarized in Figs. 5–7, which together serve to illustrate the most significant functional dependences on the orbital parameters. Solid lines in these figures represent the median uncertainties observed when ranging over parameter values *other* than the one used as abscissa in a particular graph, while dashed lines indicate the corresponding 10th and 90th percentiles of the distributions. In other words, the dashed-solid-dashed-line triplets illustrate the most probable fractional uncertainties and their ranges for 80% of the binary pulsar systems simulated. Labels on some of the curves identify some parameter values responsible for especially favorable or unfavorable measurement circumstances.

Figure 5 shows that the measurabilities of $\dot{\omega}$ and γ depend periodically on ω_0, as we have already seen for PSR's 1913+16 and 1534+12 in Figs. 3 and 4. The sharp

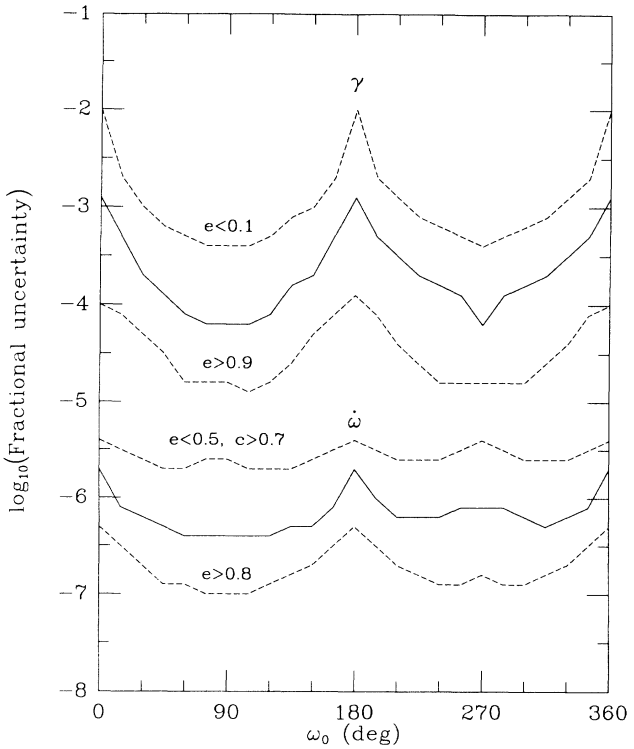

FIG. 5. Fractional uncertainties of the PK parameters $\dot{\omega}$ and γ, estimated for generic binary pulsars with 10-h orbital periods and a wide range of orbital eccentricities e and inclinations i, and plotted as a function of ω_0. Solid curves represent median uncertainties over all of the sampled values of e and $c \equiv |\cos i|$; dashed curves represent the 10th and 90th percentiles of the observed distributions. Like those illustrated in Figs. 3 and 4, these simulations assume 10 years of 2-hours-per-month observations with timing accuracies of 1 μs in 5 minutes.

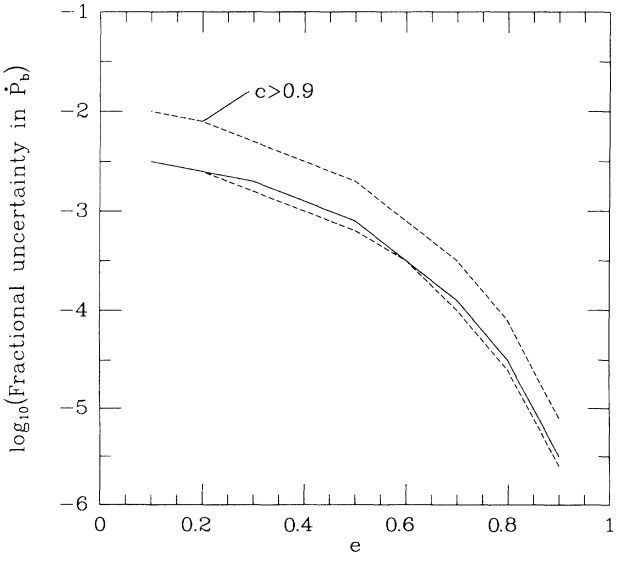

FIG. 6. Fractional uncertainties of the orbital period derivative, $\dot{P}_b$, estimated for generic binary pulsars and plotted as a function of orbital eccentricity e. See caption of Fig. 5 for further details.

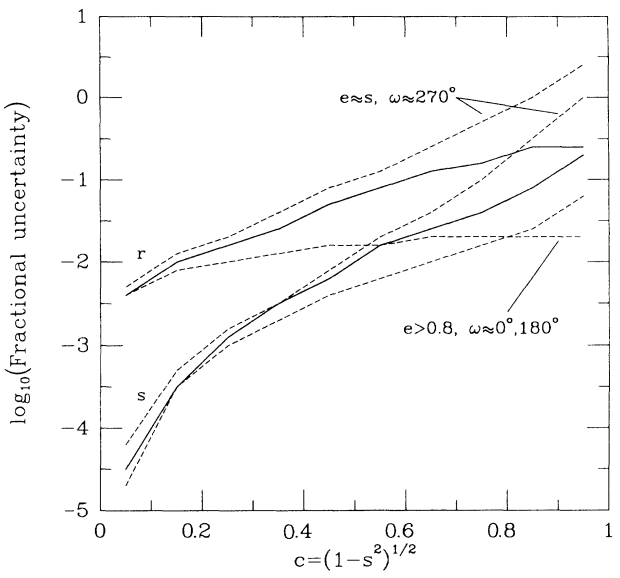

FIG. 7. Fractional uncertainties for the PK parameters r and s, estimated for generic binary pulsars and plotted as a function of $c \equiv |\cos i|$. See caption of Fig. 5 for further details.

decrease in measurability of $\dot{\omega}$, γ [and δ_θ, see Figs. 3 and 4] when $\omega_0 \approx 0°$ or 180° can be understood analytically by following the methods of [43] and [36]. Short-term fits to a DD model give access to $X = x(1-e_\theta^2)^{1/2}\cos\omega + \gamma$ and $Y = x\sin\omega$, and the secular change of ω causes the point (X,Y) to trace out an ellipse of eccentricity $e_\theta = e(1+\delta_\theta)$ centered around the point $(\gamma, 0)$. It is easy to see geometrically why the values $\omega = 0°$ or 180° render more difficult the problem of determining the center of the ellipse from a small span of data. An analytical investigation of this problem (for $\omega_0 \neq 0$, $\omega_0 \neq 180°$) leads to the scaling laws listed in columns 3 and 5 of Table II.

Several other features of the curves in Figs. 5–7 are easily recognized and readily understood. For example, we see in Fig. 5 that $\dot{\omega}$ is especially difficult to measure if $e < 0.5$ and $c > 0.7$, and that measuring γ becomes progressively more difficult for small values of e. Figure 6 shows that the measurability of $\dot{P}_b$ is strongly dependent on e and nearly independent of other parameters, unless c is close to 1 (and thus s close to 0). Finally, Fig. 7 shows that r and s are most easily measured when s is large, because the Shapiro time delay is strongest and most easily recognizable when the orbit is viewed edge-on. These parameters become particularly difficult to measure if s is small, especially if $e \approx s$ and $\omega \approx 270°$ [this feature can be understood analytically from a study of the function $\Delta_S(u)$, Eq. (2.2d)]. In general, the fractional parameter uncertainties depend on our viewing angles of the orbit in both longitude and inclination, on covariances among the parameters, and on the size of the associated post-Keplerian effects, which are often enhanced if e and s are large.

D. Measurability of pulse-structure parameters

Until now we have discussed only the measurability of the PK parameters accessible through timing observa-

tions. The best hope for gaining access to the remaining parameters is through careful measurements of the pulse shape (i.e., the phase-resolved intensity curve, modulo an overall scale factor) and details of the radio polarization. As a definite example, let us consider the favorable case where the magnetic axis of a spinning neutron star passes close to the line of sight, i.e., the case where one observes the "core emission" of the pulsar. (This case does not apply to PSR 1913+16, where the line of sight cuts across a hollow cone around the magnetic axis [63], but we argue below that it probably does apply to PSR 1534+12.) For simplicity we assume circular symmetry of the emission pattern around the magnetic axis **b**. The received intensity is then a function only of the angle θ ($\cos\theta = \mathbf{N}\cdot\mathbf{b}$, as in Sec. II B), and for small angles around **b** we have approximately

$$\frac{\theta^2}{\sin^2\alpha} = \tilde{\phi}^2 + \frac{\tilde{\beta}^2}{\sin^2\alpha} \equiv \Phi + \frac{\tilde{\beta}^2}{\sin^2\alpha}\ , \tag{4.5}$$

where α again represents the angle between the pulsar axis and the magnetic axis; $\tilde{\phi} \equiv \phi - \phi_0$ is the longitude of **b** about the pulsar axis, i.e., the rotational phase of the pulsar, with its origin at ϕ_0, the center of the pulse; $\tilde{\beta} \equiv \zeta - \alpha$ denotes the "impact parameter" of the line of sight with respect to the magnetic pole; and we introduce the shorthand notation $\Phi \equiv \tilde{\phi}^2$, to be used in the following discussion. [Do not confuse the present use of the notation $\tilde{\beta}$ with the notations $\boldsymbol{\beta} \equiv \mathbf{v}_1/c$, $\beta_1 = nx(1-e^2)^{-1/2}$, used earlier.] Under the specified assumptions the pulse shape, i.e., the normalized pulse intensity $\hat{S}(\phi) \equiv S(\phi)/S(\phi_0)$ [assuming that we have corrected for the effects of the blueshift factor $1 + \mathbf{n}\cdot\boldsymbol{\beta}$ in Eq. (2.16)], will be some fixed function of $\Phi + \tilde{\beta}^2/\sin^2\alpha$. In other words, each value of the impact parameter $\tilde{\beta}$ corresponds to a "cut" of a fixed emission pattern, and the assumed radial symmetry of this pattern permits one to reconstruct the two-dimensional beam shape from the observed one-dimensional cut.

For binary pulsars, the observed cut will vary with orbital phase because of aberration. Let us denote by $F(\Phi)$ the central cut corresponding to $\tilde{\beta} = \zeta - \alpha$, where ζ denotes, as in Eq. (2.19), the fixed (over an orbital period) angle between $\mathbf{s}_1$ and **n** [one should keep in mind Eq. (2.10b), which says that **N** oscillates during an orbital period around its average value $\langle\mathbf{N}\rangle = \mathbf{n}$]. We find that the pulse shape varies with aberration as

$$\hat{S}(\phi) = F(\Phi) + K\varepsilon G(\Phi), \tag{4.6}$$

where

$$\varepsilon = \frac{2\tilde{\beta}\delta_{\mathrm{A}}\tilde{\beta}}{\sin^2\alpha} = \frac{2\tilde{\beta}\delta_{\mathrm{A}}\zeta}{\sin^2\alpha}, \tag{4.7a}$$

$$K = -F'(0), \tag{4.7b}$$

$$G(\Phi) = F(\Phi) - F'(\Phi)/F'(0), \tag{4.7c}$$

in which $\delta_{\mathrm{A}}\zeta$ is the aberration effect given by Eq. (2.20) and the primed quantities are derivatives with respect to the convenient intermediate variable $\Phi \equiv \tilde{\phi}^2$. Starting from the observed average pulse shape, one can compute the normalized function $F(\Phi)$, $F(0) \equiv 1$ [checking in the process that, indeed, $\hat{S}(\phi)$ is nearly even around some ϕ_0], and thereby compute $G(\Phi)$ by means of Eq. (4.7c). The measurability of aberration-induced changes in the pulse shape then depends on the magnitude of $K\varepsilon$ and on the shape and maximum value of the function $G(\Phi)$.

As an example of this procedure, we computed the function G, reexpressed as a function of $\tilde{\phi}$, for the main pulse of the millisecond pulsar PSR 1937+21 (for which we had detailed, digitized pulse-shape information available). It turns out to be positive valued and consists of two humps, of height $G_{\max} = 0.20$, attaining their maximum values at $\tilde{\phi}_{\max} = \pm 1.06\tilde{\phi}_{1/2}$ [where $\tilde{\phi}_{1/2}$ denotes the half-width of the pulse at half-maximum, i.e., $F(\tilde{\phi}^2_{1/2}) = 0.5$]. More precisely, we found that on the interval $[-2\tilde{\phi}_{1/2}, +2\tilde{\phi}_{1/2}]$ the pulse shape of PSR 1937+21 is well approximated by a simple "generalized Lorentzian" curve, namely, the function

$$\hat{S}(\tilde{\phi}) = F(\tilde{\phi}^2) = [1 + \tilde{\phi}^2/a]^{-p}, \tag{4.8}$$

for a value $p \simeq 1.5$. (One would need a smaller value of p to fit the wings of the main pulse, $|\tilde{\phi}| > 2\tilde{\phi}_{1/2}$, where the falloff in intensity becomes more gradual.) Such a simple representation allows one to compute $G(\Phi)$ analytically, and by doing so one easily recovers the two-hump features quoted above, including the numerical values. It is tempting to suggest that such a simple power law is a generic feature of pulsar core emission in cases where the line of sight is known to pass near a magnetic pole, and that it may contain useful hints about the pulsar emission mechanism.

For the time being, the best binary pulsar candidate in which to detect aberration-induced changes of pulse shape seems to be PSR 1534+12. We therefore estimated in advance the probable values of some important parameters for this pulsar, using the following line of reasoning. First, we note that published data for this pulsar [41] show the existence of an interpulse. Assuming that beams from the two magnetic poles have equal intrinsic emission strength, we interpret the weaker observed intensity of the interpulse as due to a larger impact parameter, $\tilde{\beta}_{\mathrm{ip}}$, than the one for the main pulse, $\tilde{\beta}_{\mathrm{mp}}$. We transform this qualitative fact into a quantitative statement by noting that the published data show that the interpulse maximum intensity is reached, on the main pulse, at a longitude $\tilde{\phi}_* \simeq 16°$. Using our assumption of circular symmetry, $S(\phi) \propto F(\tilde{\phi}^2 + \tilde{\beta}^2/\sin^2\alpha)$, near each pole we obtain $\tilde{\beta}^2_{\mathrm{ip}} = \sin^2\alpha\tilde{\phi}^2_* + \tilde{\beta}^2_{\mathrm{mp}}$. We expect the value of $|\tilde{\beta}_{\mathrm{mp}}|$ to be comparable to the main pulse half-width at half-maximum, which is $\sim \frac{1}{2}(450\ \mu s)$, i.e., $\tilde{\phi}_{1/2} = 2.14°$ (see Ref. [41]). Using our generalized Lorentzian shape for the central part of the main pulse, i.e., an intensity proportional to $(1 + \theta^2/\sigma^2)^{-p}$, so that the quantity a appearing in Eq. (4.8) is $(\tilde{\beta}^2 + \sigma^2)/\sin^2\alpha$, we can quantitatively relate the observed $\tilde{\phi}_{1/2}$ to $\tilde{\beta}_{\mathrm{mp}}$ and the "intrinsic" width parameter σ. For $p \simeq 1.5$ this yields $(\tilde{\beta}^2_{\mathrm{mp}} + \sigma^2)^{1/2} = 2.8°$. Barring the unlikely cases where either $\tilde{\beta}_{\mathrm{mp}} \ll \sigma$ or $\tilde{\beta}_{\mathrm{mp}} \gg \sigma$, we therefore estimate that $|\tilde{\beta}_{\mathrm{mp}}| \simeq 2°$. The above reasonings tell us that α is within 9° of 90°, $|\tilde{\beta}_{\mathrm{mp}}| \simeq 2°$, and $|\tilde{\beta}_{\mathrm{ip}}| \simeq 16°$.

Information about the signs of the two impact param-

eters $\tilde{\beta}_{\rm mp}$ and $\tilde{\beta}_{\rm ip}$ is contained in polarimetry measurements. Differentiating Eq. (2.21) yields

$$(d\psi/d\tilde{\phi})_{\rm max} = \sin\alpha/\sin\tilde{\beta} \tag{4.9}$$

for the slopes of the polarization-angle curves at the center of the main pulse or interpulse [52]. From a private communication with A. Wolszczan, and after flipping the sign of the polarization angle to pass from the usual observers' convention to our theoretically preferred convention for measuring ψ, we learned that the slope $(d\psi/d\tilde{\phi})_{\rm mp} < 0$, while $(d\psi/d\tilde{\phi})_{\rm ip} > 0$. Thus the signs of the main-pulse and interpulse impact parameters are $-$ and $+$, respectively. Finally, using the equations

$$\alpha = \frac{\pi}{2} + \frac{1}{2}(\tilde{\beta}_{\rm ip} - \tilde{\beta}_{\rm mp}), \tag{4.10a}$$

$$\zeta = \frac{\pi}{2} + \frac{1}{2}(\tilde{\beta}_{\rm ip} + \tilde{\beta}_{\rm mp}), \tag{4.10b}$$

$$\lambda = \frac{\pi}{2} - \frac{1}{2}(\tilde{\beta}_{\rm ip} + \tilde{\beta}_{\rm mp}), \tag{4.10c}$$

we can determine most of the angles we need. Our final estimates based on this simplified model are

$$\tilde{\beta}_{\rm mp} = -2^\circ, \tag{4.11a}$$

$$\tilde{\beta}_{\rm ip} = +16^\circ, \tag{4.11b}$$

$$\alpha = 99^\circ, \tag{4.11c}$$

$$\zeta = 97^\circ, \tag{4.11d}$$

$$\lambda = 83^\circ. \tag{4.11e}$$

We call special attention to two consequences of Eq. (4.11e). The first is that the timing data give only access to $\sin i$ [41,42], so there is a twofold ambiguity in i: either $i = i_1 \simeq 75^\circ$, or $i = i_2 = \pi - i_1 \simeq 105^\circ$. But we expect, especially in PSR 1534+12 which has a moderate orbital eccentricity, to have only a small misalignment δ between $\mathbf{s}_1$ and $\mathbf{k}$ (see end of Sec. III B above). In other words, we expect $\lambda \simeq i$. This selects the solution $i_1 \simeq 75^\circ$ as the more probable, because it requires only $\delta \geq |\lambda - i_1| = 8^\circ$, while i_2 requires $\delta \geq |\lambda - i_2| = 22^\circ$. Finally, there still remains one unestimated angle in the problem, the longitude $\phi_{\rm SO}$ of $\mathbf{s}_1$ on its precession cone around $\mathbf{k}$, such that $\lambda - i = \delta\cos\phi_{\rm SO}$ in the small misalignment approximation of Eqs. (3.36) above. This missing information affects mainly η, the second polar angle of $\mathbf{s}_1$, given in the small misalignment approximation by $\eta + \pi/2 = \delta\sin\phi_{\rm SO}/\sin\lambda$. From $|\lambda - i| = 8^\circ$ we expect (statistically) $\delta \lesssim 16^\circ$ and therefore $|\eta + \pi/2| \lesssim 16^\circ$.

Using the published data on PSR 1534+12, as well as the various estimates described above, we can now calculate the expected effect of aberration on the angle ζ, namely,

$$\delta_{\rm A}\zeta = \delta_{\rm A}\tilde{\beta} = -[1.0C(u) + 4.0\cos\eta S(u)] \times 0.01^\circ\,. \tag{4.12}$$

We note that $|\cos\eta|$ is expected to be smaller than about $\sin 16^\circ \simeq 0.28$; from Eqs. (4.12), (4.6), and our results on the measurability of pulse-shape changes, we conclude that even if $\cos\eta = 0$, pulse-shape changes should exist at the level $|\delta_{\rm A}S| \approx 1.7 \times 10^{-3}$. Moreover, Eqs. (4.9) and (4.12) show that if our estimate $|\tilde{\beta}_{mp}| \simeq 2^\circ$ is confirmed by detailed polarization observations, the maximum slope of the polarization swing in the main pulse should vary by at least one percent over the orbital period. With special care in measurements and calibrations, such a change might be detectable in the future.

We conclude that it is important to perform high-time-resolution polarimetry of PSR 1534+12 to test our indirect estimates for $\tilde{\beta}_{\rm mp}$ and $\tilde{\beta}_{\rm ip}$, and then to plan a sequence of high-quality pulse-shape and polarimetry observations looking for the aberration effects discussed above. Such measurements would be able to (1) confirm the sign of $\cos i$ that we selected on plausibility grounds; (2) confirm our estimate for λ, the first polar angle of $\mathbf{s}_1$; and (3) give access, in a redundant way, to the second polar angle η. As we have already emphasized, knowledge of η (obtainable on a short-time scale by the method just emphasized) is a necessary prerequisite for being able to use any observation of a slow change of λ, through secular variations of either the pulse shape or the polarization angles, as evidence for spin-orbit precession and thus an important test of relativistic gravity. One should also recall that an alternative route for measuring η is to monitor the intrinsic secular variation of ψ_0, as discussed at the end of Sec. III.

V. STRONG-FIELD TESTS OF TENSOR-BISCALAR THEORIES

A. Timing predictions of tensor-biscalar theories

In previous sections we have described a purely phenomenological, theory-independent procedure for analyzing binary pulsar timing observations. We now wish to select a specific class of gravity theories, containing general relativity as a special case, and discuss the extent to which binary pulsar data could constrain them. The theories to be considered belong to the general class of tensor-multiscalar theories recently studied by Damour and Esposito-Farèse [32]. They arise naturally in current attempts toward unifying gravity with the other fundamental interactions, and/or at quantizing gravity. They are also the most natural generalizations of the well-known tensor-scalar Jordan–Fierz–Brans–Dicke theory. The latter theory has played a useful role in suggesting new tests of relativistic gravity that could be seen only when contrasting general relativity with an alternative theory. This is notably the case for tests which use as an essential ingredient the violation of the equivalence principle by self-gravity effects [5, 44]. However, present constraints on this theory from solar-system data are so tight, and the structure of the theory so rigid (only one free parameter), that it is virtually indistinguishable from general relativity in its predictions, even in the strong-field regime. By contrast, recent discussion of more general tensor-multiscalar theories [32] has shown that under some conditions [67] these theories can pass all existing solar-system tests, while still differing significantly from general relativity in the strong-field regime, and notably in their predictions for the orbital dynamics and timing behavior of binary pulsars.

We consider here a specific two-parameter subclass of tensor-multiscalar theories. This subclass is defined by having two scalar fields ϕ_1 and ϕ_2 mediating the effective gravitational interaction in addition to a tensor field $g^*_{\mu\nu}$. The action defining this class of tensor-biscalar theories reads

$$S_{\rm tot} = S_{g_*} + S_\phi + S_m \ , \tag{5.1a}$$

$$S_{g_*} = \frac{c^4}{4\pi G_*}\int \frac{\sqrt{g_*}}{c}\, d^4x\, \frac{R_*}{4} \ , \tag{5.1b}$$

$$S_\phi = -\frac{c^4}{4\pi G_*}\int \frac{\sqrt{g_*}}{c}\, d^4x\, g_*^{\mu\nu}\partial_\mu\phi_1\partial_\nu\phi_2 \ , \tag{5.1c}$$

$$S_m = S_m[\psi_m, \tilde{g}_{\mu\nu}] \ , \tag{5.1d}$$

$$\tilde{g}_{\mu\nu} \equiv \exp[2a(\phi_1,\phi_2)]g^*_{\mu\nu} \ , \tag{5.1e}$$

where

$$a(\phi_1,\phi_2) = \phi_2\left[1-\phi_1+\left(\frac{A}{B}-1\right)\phi_1^2\right] + \frac{1}{6}\beta'\phi_1^3 + \frac{1}{24}\beta''\phi_1^4 \ , \tag{5.2}$$

and β' and β'' are the two free parameters of the theory. The quantities A and B appearing in Eq. (5.2) are the pure numbers

$$A = \frac{4}{3}\left(1+\frac{2}{\pi}\int_0^\pi \frac{\sin^3 x}{x}\, dx\right) = 2.156\,917\,6 \ , \tag{5.3a}$$

$$B = \frac{4}{9}\left(2+\frac{1}{\pi}\int_0^\pi \frac{\sin^3 x}{x}\, dx\right) = 1.026\,152\,9 \ , \tag{5.3b}$$

and should not be confused with the aberration parameters of Eqs. (3.16) and (3.17).

Equation (5.1d) represents the action for the matter, with ψ_m denoting generically some material variables. It shows that we are within the framework of metric theories; the weak equivalence principle is automatically satisfied, as all non-self-gravitating test masses fall along geodesics of the "physical" metric $\tilde{g}_{\mu\nu}$ defined by Eq. (5.1e). However, the strong equivalence principle is *not* satisfied in this theory: strongly self-gravitating ("compact") bodies do not fall in the same way as ordinary bodies. Violations of the strong equivalence principle depend on the two free parameters of the theory, β' and β'', and on the compactness of the considered body, as measured by the quantity

$$c_A \equiv -2\frac{\partial \ln m_A}{\partial \ln \tilde{G}} \ . \tag{5.4}$$

In Eq. (5.4) A is a label for the considered body, m_A its inertial mass, and $\tilde{G}$ denotes the local value, at the position of the compact body, of the gravitational constant (as measured by a Cavendish experiment performed at the location of, but in absence of, the compact body). It is given by $\tilde{G} = G_*[1+2\partial_1\hat{a}\partial_2\hat{a}]\exp(2\hat{a})$, where $\partial_1 \equiv \partial/\partial\phi_1$, etc., and where $\hat{a}$ denotes the local value of $a(\phi_1,\phi_2)$, Eq. (5.2), as determined by the externally generated scalar fields $\hat{\phi}_1$ and $\hat{\phi}_2$ without the contribution of body A. At spatial infinity the scalar fields tend to zero and the locally measured value of $\tilde{G}$ tends to the constant G_* appearing in the action (5.1), which we can identify with the usual Newtonian constant G.

Let us refer to the gravity theory defined by Eqs. (5.1)–(5.3) as $T(\beta',\beta'')$. When both β' and β'' tend to zero, the predictions of the theory tend smoothly to those of general relativity, as will be apparent in the explicit formulas given below. Damour and Esposito-Farèse have worked out the consequences of generic tensor-multiscalar theories, and have shown that the special two-parameter subclass $T(\beta',\beta'')$ has the following particular properties: (1) its post-Newtonian limit coincides with that of general relativity, so that it passes all solar-system tests; (2) the dipole gravitational radiation carried away by the scalar fields in a neutron-star–white-dwarf binary system is exactly canceled at order $(v^{\rm orbit}/c)^3$, so that it passes the "4U1820−30 test" [68]; and (3) the $\dot{\omega}$-γ-$\dot{P}_b$ test for PSR 1913+16 can be satisfied for theories that are very different from general relativity. Moreover, the $T(\beta',\beta'')$ theory has some useful features of generality: the most general tensor-biscalar theory satisfying the above criteria will differ from it only in powers of the compactnesses (5.4) of higher order than those included in $T(\beta',\beta'')$. As c_A is typically $\simeq 0.3$, higher powers of c_A become quickly very small, and one can expect more general tensor-scalar theories to be practically indistinguishable from $T(\beta',\beta'')$ with respect to binary pulsar data.

The Lagrangian describing the orbital dynamics of N compact bodies has been derived in Ref. [32], and has the form of Eq. (3.1) above. The values of the strong-field-modified coefficients appearing in this Lagrangian are given by

$$G_{AB} = G_*[1+(\alpha_A\alpha_B)] \ , \tag{5.5a}$$

$$\varepsilon_{AB} = \frac{3-(\alpha_A\alpha_B)}{1+(\alpha_A\alpha_B)} \ , \tag{5.5b}$$

$$G^A_{BC} = G_*^2\{[1+(\alpha_A\alpha_B)][1+(\alpha_A\alpha_C)]+(\alpha_B\beta_A\alpha_C)\} \ , \tag{5.5c}$$

where the intermediate quantities $(\alpha_A\alpha_B)$ and $(\alpha_B\beta_A\alpha_C)$ take the following explicit form, when one uses the convenient approximate approach to the higher-order compactness parameters advocated in Ref. [32]:

$$(\alpha_A\alpha_B) = \tfrac{1}{2}\beta' B\,(c_A^2+c_B^2) \ , \tag{5.6a}$$

$$(\alpha_A\beta_B\alpha_C) = \beta'[-c_B-\tfrac{1}{2}B(c_A^2+c_C^2)+(A-3B)c_B^2-(A-B)c_B(c_A^2+c_C^2)+\tfrac{1}{2}(2A^2-7AB+5B^2)c_B^2(c_A^2+c_C^2)] + \beta'^2B^2[-3c_B^3+c_B^2(c_A^2+c_C^2)+c_B^4+\tfrac{1}{2}c_Bc_A^2c_C^2+Ac_B^2c_A^2c_C^2]+\tfrac{1}{2}\beta''Bc_B^2 \tag{5.6b}$$

It is clear from Eqs. (5.5) and (5.6) that β' parametrizes deviations from general relativity that start at order

(compactness)^2 in G_{AB} and ε_{AB}, and (compactness)^1 in $(\alpha_A\beta_B\alpha_C)$, while β'' enters only in $(\alpha_A\beta_B\alpha_C)$ at order (compactness)^2. Inserting Eqs. (5.5) and (5.6) into the results of Sec. III leads to explicit expressions, within the theory $T(\beta',\beta'')$, for the post-Keplerian timing parameters as functions of the two inertial masses. Let us write down explicitly the most important parameters:

$$k = \frac{3}{1-e^2}(nT_\odot\hat{M})^{2/3}\left(\frac{1-(\alpha_1\alpha_2)/3}{[1+(\alpha_1\alpha_2)]^{1/3}} - \frac{1}{6}\frac{X_1(\alpha_1\beta_2\alpha_1)+X_2(\alpha_2\beta_1\alpha_2)}{[1+(\alpha_1\alpha_2)]^{4/3}}\right) , \tag{5.7a}$$

$$\gamma = \frac{e}{n}(nT_\odot\hat{M})^{2/3}\frac{X_2}{[1+(\alpha_1\alpha_2)]^{1/3}}\{1+X_2[1+(\alpha_1\alpha_2)]+(\alpha_0\alpha_2)\} , \tag{5.7b}$$

$$r = T_\odot\hat{m}_2 , \tag{5.7c}$$

$$s = \frac{xn^{2/3}}{(T_\odot\hat{M})^{1/3}}\frac{1}{X_2[1+(\alpha_1\alpha_2)]^{1/3}} , \tag{5.7d}$$

$$[\delta_\theta^{\rm obs}]_{\|} = (nT_\odot\hat{M})^{2/3}[1+(\alpha_1\alpha_2)]^{2/3}\left(\frac{4}{1+(\alpha_1\alpha_2)} - X_1X_2 - \frac{1}{2}X_1^2 - \rho X_2^2\right) - \frac{n\gamma}{e} + \varepsilon_{A_0} . \tag{5.7e}$$

In Eqs. (5.7) a caret over the masses, e.g., $\hat{M} \equiv \hat{m}_1 + \hat{m}_2$, means that they are expressed in solar-mass units; we have also introduced a shorthand for the solar mass in time units, $T_\odot \equiv GM_\odot c^{-3} = 4.925\,490\,947\ \mu s$. The extra contribution $\kappa\eta^*$ in Eq. (3.11) does not appear in Eq. (5.7b) because η^* turns out to be zero in $T(\beta',\beta'')$. In Eq. (5.7e) we have assumed for definiteness that the pulsar spin axis was aligned with the angular momentum ("parallel case," hence the subscript $\|$). The quantity ρ is an abbreviation for the dimensionless ratio of Keplerian parameters, $\rho = P_bP_p/[4\pi^2x^2(1-e^2)^{1/2}]$, and ε_{A_0} denotes, as in Eq. (3.18) above, some fiducial value of the aberration parameter (usually chosen as the value expected in general relativity computed from the observed values of $\dot{\omega}$ and γ, assuming the parallel case). Also note that in Eq. (5.7e) γ represents the entire right-hand side of Eq. (5.7b). Conspicuously absent from the list (5.7) of important parameters is the theoretical prediction within $T(\beta',\beta'')$ for $\dot{P}_b$. It has been worked out in Ref. [32], and we shall use their results in drawing Figs. 8(b) and 9 below.

The spin-orbit coupling coefficients Γ_A^B have not been worked out in tensor-multiscalar theories, but their values will not be needed for the effects discussed below. We will, however, need to know how the compactness of body A, Eq. (5.4), varies with its inertial mass m_A. This variation depends on the equation of state of the nuclear matter comprising the neutron star. In view of the rather large uncertainties concerning this equation of state, we shall follow Ref. [32] and adopt a simplified approach in which c_A is proportional to m_A. (It was shown in Ref. [32] that this relation provides surprisingly good fits to the numerical results obtained when using a broad sample of equations of state.) The remaining dependence on the nuclear equation of state is entirely contained in the slope c_A/m_A, for which we shall adopt the median value among the fits in Ref. [32] to a sample of four representative equations of state. This means that we shall take

$$c_A = 0.21\,\hat{m}_A , \tag{5.8}$$

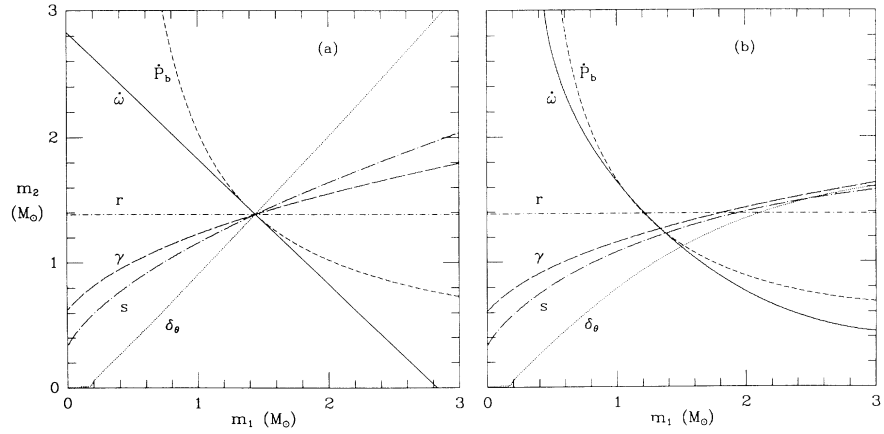

FIG. 8. Theoretical curves in the m_1-m_2 plane corresponding to the same set of six mock "observed" PK parameters, analyzed within the framework of two different theories. In (a) the general-relativistic formulas were used; convergence of the six curves at one point was guaranteed by having chosen PK parameter values consistent (within general relativity) with the values of $\dot{\omega}$, γ, and the Keplerian parameters observed for the PSR 1913+16 system [22, 23]. In (b) the same parameter values were analyzed within the tensor-biscalar theory $T(3,7)$. Note that although most of the curves are substantially modified in (b), those for $\dot{\omega}$, γ, and $\dot{P}_b$ still pass (almost) through a single point. In both (a) and (b) we used $\varepsilon_{A_0} \equiv 4.983 \times 10^{-6}$ when constructing the δ_θ curves.

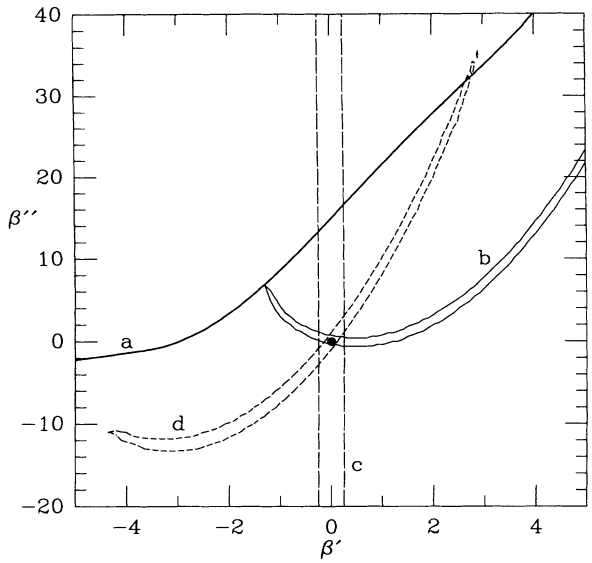

FIG. 9. Combined theory-dependent analysis of published observations of the binary pulsars PSR 1913+16 and PSR 1953+29, and simulated observations of PSR 1534+12, within the framework of a two-parameter family of tensor-biscalar theories $T(\beta', \beta'')$. Values of β' and β'' lying above curve (a) are ruled out because they are inconsistent with the observed values of $\dot{\omega}$, γ, and the Keplerian parameters for PSR 1913+16. Contour (b) illustrates the 90% confidence region for $\chi^2(\beta', \beta'')$, based on observations of PSR 1913+16 taken through December 1990. Vertical dashed lines (c) represent boundaries of the 90% confidence region defined by lack of evidence for violation of the strong equivalence principle in the orbital data for PSR 1953+29. Finally, contour (d) illustrates a hypothetical 90% confidence region based on simulated observations of PSR 1534+12 (3 years of 2-hours-per-month observations with 1 μs accuracy in 5 minutes). The available parameter space for viable theories is the intersection of all the allowed regions [recall, however, that the contour (d) is presently hypothetical]. The central dot at $\beta' = \beta'' = 0$ corresponds to general relativity.

where $\hat{m}_A$ is the mass m_A in solar units.

With the help of Eqs. (5.6)–(5.8), we can now give an explicit illustration of the type of test made possible by measurements of many PK parameters. Let us consider a mock set of PK parameters consisting of the values of $\dot{\omega}$ and γ actually measured in the PSR 1913+16 system, and the values of $\dot{P}_b$, r, s, and δ_θ expected to be observed if general relativity is correct (i.e., computed from $\dot{\omega}$, γ, and the measured Keplerian parameters by using general-relativistic formulas). Then, by construction, these mock parameters and the theory $T(0,0)$ (i.e., general relativity) define a set of curves in the mass plane which necessarily meet at one point, as illustrated in Fig. 8(a). This graph may be compared with Fig. 9 of Ref. [22], which was based on real measurements of PK parameters. For clarity, in Fig. 8 we have not included any indication of experimental uncertainties, which for r, s, and δ_θ would be quite large with the presently available data quality.

By contrast, Fig. 8(b) shows the curves defined by Eqs. (5.7) when analyzing the same set of phenomenological parameters within the framework of a different theory of gravity, namely the particular tensor-biscalar theory $T(3,7)$. Of particular interest is the fact that the three curves defined by $\dot{\omega}$, γ, and $\dot{P}_b$, although appreciably displaced by strong-field effects from their positions in Fig. 8(a), still meet approximately at one point (within one standard deviation) while the other curves do not (see Ref. [32] for further discussion). This phenomenon illustrates the importance of completing the presently available $\dot{\omega}$-γ-$\dot{P}_b$ test by new strong-field tests based on measurements of r, s, and δ_θ.

B. Binary pulsar tests of tensor–biscalar theories

Analyzing pulsar data in a theory-dependent manner, rather than in the purely phenomenological way described above, can be interesting for two reasons. First, when precise measurements have determined a set of phenomenological parameters, a theory-dependent approach helps to elucidate the physical meaning of these measurements and to transform them into explicit quantitative limits on possible strong-field deviations from the correct theory of gravity. Second, it provides a common ground for intercomparing the quality and strength of tests performed by measuring different PK parameters in data coming from different pulsars. Another interest of a theory-dependent approach will be illustrated in a subsequent paper [42], and consists of trading, in favorable cases, some weak constraints on a manifold of generic theories for stronger constraints on a more restricted class of theories.

In the present paper we shall illustrate the utility of complementing the phenomenological PPK approach with a theory-dependent one by analyzing published or numerically simulated data for three different pulsars, using the framework of a specific two-parameter theory, $T(\beta', \beta'')$. The use of a family of theories parametrized by several real parameters plays an important role: it provides a continuous (in our case two-dimensional) space of possible theories, within which experimental data can provide quantitative constraints in the form of visualizable "allowed regions." In the familiar weak-field PPN framework, the parameters β, γ, . . . , played dual roles as both phenomenological parameters and theory parameters. In our present work these two roles have been separated: the PK parameters provide a means for phenomenological analysis of the experimental data, while the theory parameters β' and β'' acquire their own distinct identities.

There are two straightforward ways in which one can pass from the phenomenological to the theory-based approach. The simplest method starts with the set of observed PK parameters $\{p^{\rm obs}\}$ and their standard deviations $\{\sigma_p^{\rm obs}\}$. Assuming for simplicity that among this set two parameters, say $\dot{\omega}$ and γ, have been measured with much higher precision than the others, one can use the theoretical predictions for these two, say Eqs. (5.7a) and (5.7b), to compute the masses m_1 and m_2 in terms of the measured values of $\dot{\omega}$, γ, and assumed values for

the theory parameters β' and β''. This first step already allows one to eliminate as nonviable any region(s) of theory space for which the two equations (5.7a) and (5.7b) cannot be satisfied simultaneously for *any* positive values of the masses. The solutions for m_1 and m_2 in terms of β' and β'' are then substituted into the theoretical expressions for each additional measured PK parameter, say Eqs. (5.7c)–(5.7d). The phenomenologically measured parameter values and standard deviations then define allowed strips in the two-dimensional theory space. [In the general case of an n-dimensional theory space, each further PK parameter measurement ($p^{\rm obs}$, $\sigma_p^{\rm obs}$) would define a thickened hypersurface, instead of a strip.]

Such a procedure is simple to implement and easy to understand (see, e.g., [32] for several uses of it), but it is only approximate because it neglects all correlations between the measured parameters. This deficiency leads us to seek a second, more satisfactory way of passing from a phenomenological to a theory-based analysis.

In terms of the general approach to measurability described in Sec. IV above, the best way to compare observational data with the predictions of some theory is to study the variation of the goodness-of-fit statistic χ^2, Eq. (4.2). For given (real or simulated) observations and a given theory, say $T(\beta',\beta'')$, the quantity χ^2 is, on using Eqs. (5.6)–(5.8) and the corresponding theoretical prediction for $\dot{P}_b$ from [32], a function of the masses m_1 and m_2, the theory parameters β' and β'', and the Keplerian parameters. Since we wish to obtain limits on the theory parameters, we first minimize χ^2 by adjusting the masses and the Keplerian parameters, and then study the variation of the resulting minimum $\chi^2(\beta',\beta'')$ when β' and β'' are varied. Level contours of $\Delta\chi^2(\beta',\beta'') \equiv \chi^2(\beta',\beta'') - \chi^2_{\rm min}$ (where $\chi^2_{\rm min}$ is the global minimum of χ^2) then define "allowed regions" of theory space with well determined confidence limits. For example, the contour $\Delta\chi^2 = 4.61$ encloses a 90% confidence region for β' and β''.

The advantages of such an analysis are several. First, it rigorously and automatically accounts for any correlations between the experimentally measured parameters. Our simulations described above show this to be particularly important for present attempts to measure r and s for PSR 1534+12: with existing data quality, these PK parameters are not expected to be separately measurable with small error bars. Nevertheless, a multiparameter χ^2 analysis should still provide strong constraints on the possible values of the pair (r,s), and therefore also on the theory parameters β',β''. A second advantage of the $\chi^2(\beta',\beta'')$ approach is that theory-based conclusions based on observations of different pulsars can be readily combined by representing in the common theory space (here the β', β'' plane) the rigorous 90% confidence regions corresponding to each test. The correct theory of gravity [if it belongs to the class $T(\beta',\beta'')$] will necessarily belong to the intersection of all such allowed regions.

Such a combination of different real and potential constraints on gravitation theories is illustrated in Fig. 9, bringing together analyses of real or simulated observations of three binary pulsars. The heavy line labeled (a) in the figure represents the "self-consistency" constraint discussed above: for the PSR 1913+16 data set, values of β' and β'' above and to the left of this curve are prohibited. A reanalysis of published observations of PSR 1913+16, following the prescription just described, produced the 90% confidence closed-contour region labeled (b). The vertical strip labeled (c) corresponds to 90% confidence bounds on β' derived from orbital data [69] on the "nonrelativistic" binary pulsar PSR 1953+29, based on its failure to violate the strong equivalence principle [39]. Finally, our simulated observations of PSR 1534+12 (in this case using just 3 years of 2-hours-per-month observing with timing uncertainties of 1 μs in 5 minutes) yield the the 90% confidence region labeled (d) in Fig. 9, and help to illustrate the real constraints that should be possible within a few years. Note that the limit (c) is somewhat different in nature from the others: as emphasized in Ref. [39], it contains some extra probabilistic assumptions, and moreover it was obtained by using the first, simple-minded, way indicated above for a theory-based analysis. In a subsequent paper [42] we shall discuss the actual limits on tensor-biscalar theories already obtainable from combining real timing observations of PSR 1534+12 with updated observations of PSR 1913+16.

VI. CONCLUSIONS AND PROSPECTS

The main aim of this paper has been to discuss how binary pulsar data can be used for experimental tests of the strong-field regime of relativistic gravity. We first presented (in Sec. II) a full account of the parametrized post-Keplerian formalism, a procedure for purely phenomenological analysis of binary pulsar data. Our analysis showed that in principle one can extract from pulsar data, in a theory-independent way, as many as 19 post-Keplerian parameters carrying dynamical information about the orbit and the spin of a neutron star and their evolution. Eight of these PK parameters, $\{k,\gamma,\dot{P}_b,r,s,\delta_\theta,\dot{e},\dot{x}\}$, are contained in pulsar timing data, while the other eleven, $\{\lambda,\dot{\lambda},\kappa,\dot{\kappa},\sigma,\dot{\sigma},\dot{\psi}_0,\kappa',\sigma',\dot{\kappa}',\dot{\sigma}'\}$, are contained in pulse structure data. To elucidate the theoretical content of the PK parameters, in Sec. III we used the framework of generic boost-invariant gravity theories to derive expressions linking these parameters to the easily measured Keplerian parameters, x, e, and P_b, the inertial masses m_1, m_2 of the pulsar and its companion, and the two polar angles defining the direction of the pulsar spin axis, λ and η. These formulas show explicitly that in a generic theory the functions $p_i^{\rm PK} = f_i^{\rm theory}(p^K, m_1, m_2, \lambda, \eta)$ contain strong-gravitational-field effects. The main conclusion of this analysis is therefore that, in principle, binary pulsar data can give access to $19-4=15$ tests of strong-field gravity (the subtraction of 4 corresponding to the four unknown physical parameters m_1, m_2, λ, and η). At present just one such test has been performed, combining $\dot{\omega}$, γ, and $\dot{P}_b$ as determined from observations of PSR 1913+16. While this test is an extremely important one, we have emphasized that it inextricably mixes strong-field and radiative effects, and therefore could, in

principle, be satisfied by an incorrect theory that has (from a general-relativistic point of view) perversely compensating behavior in these two regimes.

We then explored in a quantitative way, in Sec. IV, the practical prospects for extracting more of the 15 possible tests from pulsar data. We evaluated the measurability of timing PK parameters by using numerically simulated observations covering a wide variety of possible binary pulsar systems. Some of the simulations mimicked known pulsars with improved, probably achievable, timing accuracies, while others were designed to mimic binary pulsars that might be discovered in the future. Our most important conclusion from the simulations is that with the present level of timing accuracy, the recently discovered binary pulsar PSR 1534+12 should already give access to two new tests of relativistic gravity if the observations are analyzed in the way emphasized in this paper. The new tests are obtainable by combining phenomenological measurements of the parameters $\dot{\omega}$, γ, r, and s — and they probe quasistationary strong-field effects *without* mixing of radiative effects. We emphasize the importance of trying to measure enough parameters, through timing or pulse-structure observations, to gain access to the longitude η in the plane of the sky of the pulsar spin axis with respect to the ascending node. In absence of such knowledge, a conclusive test of relativistic precession of the pulsar spin will not be possible. Another conclusion is that PSR 1913+16 could give access to three further tests, beyond the presently obtained $\dot{\omega}$-γ-$\dot{P}_b$ test, through measurements of r, s, and δ_θ. Separated measurements of r and s would become possible with interesting accuracy if a suitable upgrading of observing techniques improved the timing accuracy by about a factor of 10, and δ_θ will be measurable within 20 years even without improvement in timing accuracy.

In Sec. V we shifted from a phenomenological to a theory-dependent analysis of binary pulsar data. For this purpose we used a two-parameter class of tensor-biscalar gravity theories. We showed how such an analysis provides a common ground for interpreting and intercomparing tests coming from observations of different pulsars. In particular, we illustrated how such a combination of independent tests can lead to very tight quantitative constraints on possible strong-field deviations from the correct theory of gravity.

ACKNOWLEDGMENTS

We thank Gilles Esposito–Farèse for help in transforming the analytical results of [32] into FORTRAN code and Joel Weisberg for helpful comments following a very thorough reading of our manuscript. J.H.T. thanks the Institut des Hautes Etudes Scientifiques for hospitality while this paper was being written, and the U.S. National Science Foundation for many years of support.

APPENDIX: GLOSSARY OF FREQUENTLY USED NOTATION

For the convenience of the reader we gather below some of the notations used most frequently in the text, especially those liable to be confused with one another. For definitions and conventions concerning angular quantities, see also Fig. 1.

a_1 Semimajor axis of pulsar orbit about the center of mass (index 1 refers to the pulsar, index 2 to the companion star)

a_R Semimajor axis of the relative orbit

A Subscript used to denote an effect of aberration, as in Δ_A, $\delta_A\zeta$, $\delta_A\psi_0$

A, B Coefficients of the aberration term Δ_A in the timing formula [Eqs. (2.2), (3.16), (3.17)]

A, B, C Labels for members of a gravitationally interacting system of N bodies [$A, B = 1, 2$ if $N = 2$, as in Eq. (3.6b)]

A, B Pure numbers $A = 2.156\,9\ldots$, $B = 1.0261\ldots$, defined in Eqs. (5.3)

$A_e(u)$ True anomaly of a pulsar's orbital motion, Eq. (2.3c)

$\mathbf{b}(T)$ Rotating unit vector directed along a pulsar's magnetic axis

B Blueshift factor used in Sec. II B and defined in Eq. (2.10a)

c Velocity of light in formulas such as (3.8b), (3.14), and (3.34)

c Shorthand for $|\cos i| = \sqrt{1 - s^2}$, used in Sec. IV and Figs. 5–7

c_A Compactness of body A, Eqs. (5.4) and (5.8)

$C(u)$ Function defined in Eq. (2.14a), used in specifying a pulsar's orbital velocity

D Doppler factor used in Secs. II A and III B

e Eccentricity of a pulsar's orbital motion, as defined in a relativistic timing model

G Newton's gravitational constant

$\mathcal{G} = G_{12}$ Strong-field modified gravitational constant for interaction between a pulsar and its companion

i Inclination between orbital plane and plane of sky ($i = 90°$ for edge-on view)

$\mathbf{i} = \mathbf{I}$ Unit vector pointing toward ascending node of orbit (see Fig. 1)

k Fractional periastron advance during one orbit, $k \equiv \dot{\omega} P_b / 2\pi$

$\mathbf{k}$ Unit vector in direction of orbital angular momentum (see Fig. 1)

$\mathbf{K} = \mathbf{K}_0$ Unit vector pointing from Earth toward pulsar system (see Fig. 1)

m_1, m_2 Masses of a pulsar and its companion, respectively

M Total mass of binary pulsar system, $M = m_1 + m_1$

n Orbital frequency or "mean motion," $n = 2\pi/P_b$

$\mathbf{n}$ Unit vector in fixed direction from pulsar toward Earth, $\mathbf{n} = -\mathbf{K}$

$\mathbf{N}$ Unit vector in direction of emission, in the pulsar comoving frame, of radio waves received at Earth; differs slightly from $\mathbf{n}$ because of aberration, Eq. (2.10b)

P_b Orbital period of binary system (periastron to periastron, at epoch T_0)

P_p Pulsar period

r Range of Shapiro time delay Δ_S, Eq. (2.2d)

$s \equiv \sin i$ Shape of Shapiro time delay Δ_S, Eq. (2.2d)

$\mathbf{s}_1, \mathbf{s}_2$ Unit vectors along the spin angular momenta of the pulsar and its companion, respectively

$S(u)$ Function defined in Eq. (2.14b), used in specifying a pulsar's orbital velocity

T Time measured in proper reference frame of a pulsar, Sec. II A

T Total time spanned by a set of pulsar timing observations, Sec. IV C

x Projected semimajor axis of a pulsar's orbit in time units, $x = a_1 \sin i/c$

X_1, X_2 Mass fractions m_1/M and m_2/M, respectively

α Fixed angle between a pulsar's spin axis $\mathbf{s}_1$ and its rotating magnetic axis, $\mathbf{b}(T)$

β Subscript used to denote quantities that vary because of aberration, e.g., ζ_β in Eq. (2.19)

α_A, β_A Tensor-multiscalar theoretical quantities appearing in the orbital Lagrangian, [Eqs. (5.5), (5.6)]

$\boldsymbol{\beta}$ Dimensionless orbital velocity of a pulsar, $\boldsymbol{\beta} = \mathbf{v}_1/c$

β_1 Orbital velocity parameter $\beta_1 = nx(1 - e^2)^{-1/2}$, as defined in Eq. (2.14c)

β_O Dimensionless relative orbital velocity, defined in Eq. (3.8b)

$\tilde{\beta}$ Angular impact parameter of line of sight with respect to rotating magnetic axis, $\tilde{\beta} \equiv \zeta - \alpha$

β', β'' Free parameters in tensor-biscalar theories

γ Parameter measuring time dilation effects, Eq. (2.2c)

δ Shorthand notation used in Sec. III B, $\delta \equiv n\gamma/e$

δ Misalignment angle between pulsar spin axis and orbital angular momentum

δ_r, δ_θ Dimensionless parameters quantifying relativistic deformations of orbit

$\varepsilon = \varepsilon_{12}$ Strong-field-modified coefficient in the generic boost-invariant Lagrangian, Eq. (3.5b)

$\varepsilon_A, \varepsilon_{A_0}$ Dimensionless aberration parameters $\varepsilon_A \equiv A/x$, $\varepsilon_{A_0} \equiv A_0/x$

ζ Angle between a pulsar's spin axis and direction from pulsar to Earth, $\zeta \equiv \pi - \lambda$ [see Figs. 1(a), 1(b)]

η Longitude of pulsar spin axis in plane of sky, measured from ascending node (see Fig. 1)

κ, κ' Post-Keplerian parameters related to pulse structure, Eqs. (2.27a), (2.28a)

λ Angle between a pulsar's spin axis and line of sight from Earth to pulsar, $\lambda \equiv \pi - \zeta$ [see Figs. 1(a), 1(b)]

μ Reduced mass, $\mu = m_1 m_2/M$

ν Shorthand notation used in Sec. III, $\nu \equiv \mu/M = X_1 X_2 = m_1 m_2/M^2$

ν Frequency of radio waves, used in some formulas of Sec. II B

ν_p Pulsar frequency, $\nu_p = 1/P_p$

ξ Strong-field-modified coefficient in the generic boost-invariant Lagrangian, Eq. (3.6a)

σ, σ' Post-Keplerian parameters related to pulse structure, Eqs. (2.27b), (2.28b)

$\sigma_A, \sigma_1, \sigma_2$ Coefficients in the spin-orbit Lagrangian, Eqs. (3.5)–(3.7)

σ_i^{obs} Observational uncertainty of ith arrival time measurement

ϕ Pulsar phase ($= \phi_0$ at center of main pulse)

ψ Linear polarization angle ($= \psi_0$ at center of main pulse)

ω Argument of periastron, i.e., angle between ascending node and direction of periastron

$\dot{\omega}$ Secular advance of periastron, $\dot{\omega} = nk = 2\pi k/P_b$

Ω Longitude of ascending node in plane of sky (see Fig. 1)

Ω_1^{spin} Precession of pulsar spin axis caused by spin-

orbit coupling; note that $\Omega_1^{\rm spin} = |\Omega_1^{\rm spin}|$ is also used

$\Omega_1^{\rm orbit}$ Vectorial angular velocity of the entire orbit caused by spin-orbit coupling

$\Omega_O^{\rm orbit}$ Vectorial angular velocity of the entire orbit caused by relativistic orbital effects

[1] R.A. Hulse and J.H. Taylor, Astrophys. J. Lett. **195**, L51 (1975).
[2] L.I. Schiff, Phys. Rev. Lett. **4**, 215 (1960).
[3] I.I. Shapiro, Phys. Rev. Lett. **13**, 789 (1964).
[4] R. Baierlein, Phys. Rev. **162**, 1275 (1967).
[5] K. Nordtvedt, Phys. Rev. **170**, 1186 (1968).
[6] K. Nordtvedt, Phys. Rev. D **3**, 1683 (1971).
[7] C.M. Will, Astrophys. J. **169**, 141 (1971).
[8] K. Nordtvedt and C.M. Will, Astrophys. J. **177**, 775 (1972).
[9] P. Jordan, Nature (London) **164**, 637 (1949); *Schwerkraft und Weltall* (Vieweg, Braunschweig, 1955); Z. Phys. **157**, 112 (1959).
[10] M. Fierz, Helv. Phys. Acta **29**, 128 (1956).
[11] C. Brans and R.H. Dicke, Phys. Rev. **124**, 925 (1961).
[12] A.S. Eddington, *The Mathematical Theory of Relativity* (Cambridge University Press, London, 1922).
[13] K. Nordtvedt, Phys. Rev. **169**, 1017 (1968).
[14] C.M. Will, Astrophys. J. **163**, 611 (1971).
[15] C.M. Will and K. Nordtvedt, Astrophys. J. **177**, 757 (1972).
[16] C.M. Will, *Theory and Experiment in Gravitational Physics* (Cambridge University Press, Cambridge, England, 1981).
[17] I.I. Shapiro, in *General Relativity and Gravitation, 1989*, edited by N. Ashby, D.F. Bartlett, and W. Wyss (Cambridge University Press, Cambridge, England, 1990), pp. 313-330.
[18] J.H. Taylor, R.A. Hulse, L.A. Fowler, G.E. Gullahorn, and J.M. Rankin, Astrophys. J. Lett. **206**, L53 (1976).
[19] J.H. Taylor, L.A. Fowler, and P.M. McCulloch, Nature (London) **277**, 437 (1979).
[20] J.H. Taylor and J.M. Weisberg, Astrophys. J. **253**, 908 (1982).
[21] J.M. Weisberg and J.H. Taylor, Phys. Rev. Lett. **52**, 1348 (1984).
[22] J.H. Taylor and J.M. Weisberg, Astrophys. J. **345**, 434 (1989).
[23] J.H. Taylor and J.M. Weisberg (unpublished data).
[24] P.C. Peters and J. Mathews, Phys. Rev. **131**, 435 (1963).
[25] T. Damour and N. Deruelle, Phys. Lett. **87A**, 81 (1981).
[26] T. Damour, C. R. Acad. Sci. Paris **294**, série II, 1355 (1982).
[27] T. Damour, in *Gravitational Radiation*, edited by N. Deruelle and T. Piran (North-Holland, Amsterdam, 1983), pp. 59-144.
[28] T. Damour, Phys. Rev. Lett. **51**, 1019 (1983).
[29] T. Damour and J.H. Taylor, Astrophys. J. **366**, 501 (1991).
[30] C.M. Will and D.M. Eardley, Astrophys. J. Lett. **212**, L91 (1977).
[31] J.M. Weisberg and J.H. Taylor, Gen. Relativ. Gravit. **13**, 1 (1981).
[32] T. Damour and G. Esposito-Farèse (unpublished).
[33] T. Damour and R. Ruffini, C. R. Acad. Sci. Paris, **279**, série A, 971 (1974).
[34] L.W. Esposito and E.R. Harrison, Astrophys. J. Lett. **196**, L1 (1975).
[35] B.M. Barker and R.F. O'Connell, Astrophys. J. Lett. **199**, L25 (1975).
[36] T. Damour and N. Deruelle, Ann. Inst. Henri Poincaré A **44**, 263 (1986).
[37] T. Damour, in *General Relativity and Relativistic Astrophysics*, Proceedings of the 2nd Canadian Conference, Toronto, Canada, 1987, edited by A. Coley, C. Dyer, and T. Tupper (World Scientific, Singapore, 1988), pp. 315–334.
[38] T. Damour and G. Schäfer, Nuovo Cimento B **101**, 127 (1988).
[39] T. Damour and G. Schäfer, Phys. Rev. Lett. **66**, 2549 (1991).
[40] S.B. Anderson, P.W. Gorham, S.R. Kulkarni, T.A. Prince, and A. Wolszczan, Nature (London) **346**, 42 (1990).
[41] A. Wolszczan, Nature (London) **350**, 688 (1991).
[42] J.H. Taylor, A. Wolszczan, T. Damour, and J. M. Weisberg, Nature (London) **355**, 132 (1992).
[43] R. Blandford and S.A. Teukolsky, Astrophys. J. **205**, 580 (1976).
[44] D.M. Eardley, Astrophys. J. Lett. **196**, L59 (1975).
[45] R. Epstein, Astrophys. J. **216**, 92 (1977); **231**, 644(E) (1979).
[46] M.P. Haugan, Astrophys. J. **296**, 1 (1985).
[47] T. Damour and N. Deruelle, Ann. Inst. Henri Poincaré A **43**, 107 (1985).
[48] N.D. Hari Dass and V. Radhakrishnan, Astrophys. Lett. **16**, 135 (1975).
[49] L.L. Smarr and R. Blandford, Astrophys. J. **207**, 574 (1976).
[50] The (nearly) constant velocity of the center of mass of the binary system with respect to the solar system adds only constant, and therefore unobservable, extra contributions in Eqs. (2.10a) and (2.10b).
[51] V. Radhakrishnan and D.J. Cooke, Astrophys. J. Lett. **3**, 225 (1969).
[52] R.N. Manchester and J.H. Taylor, *Pulsars* (Freeman, San Francisco, 1977).
[53] K. Nordtvedt, Astrophys. J. **297**, 390 (1985).
[54] H.W. Woodcock and P. Havas [Phys. Rev. D **6**, 3422 (1972)] and H. W. Woodcock [*ibid.* **17**, 1539 (1978)] have pointed out the possibility of having some "asymmetric" contributions in the most general Poincaré-invariant Lagrangian. Such terms do not appear, however, in generic tensor-multiscalar field theories [32], and we shall not include them here.
[55] W. Tulczyjew, Acta Phys. Pol. **18**, 37 (1959).
[56] B.M. Barker and R.F. O'Connell, Phys. Rev. D **12**, 329 (1975).
[57] B.M. Barker and R.F. O'Connell, Phys. Rev. D **14**, 861 (1976).

[58] G. Börner, J. Ehlers, and E. Rudolph, Astron. Astrophys. **44**, 417 (1975).
[59] C.F. Cho and N.D. Hari Dass, Ann. Phys. (N.Y.) **96**, 406 (1976).
[60] T. Damour, in *Physics and Astrophysics of Neutron Stars and Black Holes*, Proceedings of the International School of Physics "Enrico Fermi," Verenna, Italy, 1975, edited by R. Giacconi and R. Ruffini, Enrico Fermi Course LXV (North-Holland, Amsterdam, 1978), pp. 547–549.
[61] L. Landau and E. Lifchitz, *Mécanique* (Mir, Moscow, 1982).
[62] T. Damour, G.W. Gibbons, and J.H. Taylor, Phys. Rev. Lett. **61**, 1151 (1988).
[63] J.M. Weisberg, R.W. Romani, and J.H. Taylor, Astrophys. J. **347**, 1030 (1989).
[64] J.M. Cordes, I. Wasserman, and M. Blaskiewicz, Astrophys. J. **349**, 546 (19^^).
[65] A.G. Lyne and R.N. Manchester, Mon. Not. R. Astron. Soc. **234**, 477 (1988).
[66] B. Lévine, *Fondements Théoriques de la Radiotechnique Statistique* (Mir, Moscow, 1973), Vol. II.
[67] In particular, the quadratic form giving the kinetic terms of the scalar degrees of freedom must be of indefinite sign, which means that at least one scalar radiative mode must carry negative energy. Note, however, that the net energy flux emitted by binary systems is generically positive, even for systems containing compact objects.
[68] C.M. Will and H. W. Zaglauer, Astrophys. J. **346**, 366 (1989). This test consists of deriving a rather stringent limit on the amount of dipole gravitational radiation emitted by a binary system containing bodies of very different compactness, e.g., a neutron star and a white dwarf. It assumes that the 11-min periodicity in the x-ray source 4U1820−30 comes from such an orbital motion.
[69] L.A. Rawley, J.H. Taylor, and M.M. Davis, Nature (London) **319**, 383 (1986).